MCTP1 promotes SNAI1-driven neuroendocrine differentiation and epithelial-to- mesenchymal transition of prostate cancer enhancement by ZBTB46/FOXA2/HIF1A

Yen-Nien Liu
Taipei Medical University
Wei-Yu Chen
Taipei Medical University
Hsiu-Lien Yeh
National Tsing Hua University
Wei-Hao Chen
Taipei Medical University
Kuo-Ching Jiang
Taipei Medical University
Han-Ru Li
Taipei Medical University
Van Thi Ngoc Tram
Taipei Medical University
Phan Vu Thuy Dung
Taipei Medical University
Zi-Qing Chen
Taipei Medical University
Michael Hsiao
Academia Sinica
Jiaoti Huang
Duke University Medical Center
Yu-Ching Wen (95207@w.tmu.edu.tw)
TMU Research Center of Urology and Kidney, Taipei Medical University

Research Article

Keywords: MCTP1, ZBTB46, FOXA2, HIF1A, SNAI1

Posted Date: June 2nd, 2022

DOI: https://doi.org/10.21203/rs.3.rs-1709799/v1

Abstract

Background

Prostate cancer (PCa) patients with bone metastases frequently exhibit abnormal calcium homeostasis. However, the molecular mechanisms underlying bone metastasis mediated by activated calcium transport signaling remain unclear. Our results showed that androgen deprivation therapy (ADT) of PCa upregulates a calcium sensor transmembrane protein, the multiple C2 domains transmembrane protein 1 (MCTP1), which is upregulated by hypoxia-induced ZBTB46/FOXA2/HIF1A signaling and is associated with SNAI1-driven neuroendocrine (NE) differentiation (NED) and epithelial-to-mesenchymal transition (EMT) in PCa.

Methods

Hypoxia induced interactions between ZBTB46, HIF1A, and FOXA2 were confirmed by immunoprecipitation (IP)-Western Blot (WB). Correlation between MCTP1 and ZBTB46/FOXA2/HIF1A complexes was analyzed by immunohistochemical (IHC) staining in consecutive tissue sections of PCa tissue microarray (TMA) comprising primary PCa and small cell PCa (SCPC) samples. The regulatory network between *MCTP1* and the hypoxia-induced ZBTB46/FOXA2/HIF1A axis was investigated by chromatin IP (ChIP)-Seq analysis, ChIP assay, and promoter reporter assays. The effect of MCTP1 on SNAI1 expression driving NED and EMT in PCa was identified in PCa cell lines using mimic hypoxia, ADT, or long-term androgen receptor (AR) antagonist culture systems. Activation of the MCTP1-mediated calcium-related pathway induces SNAI1-driven NED and aggressive progression of PCa under hypoxic conditions was examined by Fluo-8 AM staining combined with flow cytometry, migration, invasion, and xenograft model validation.

Results

MCTP1 is highly expressed in advanced PCa tissues and is associated with ZBTB46/FOXA2/HIF1A abundance. Upregulation of MCTP1 enhances SNAI1-mediated cell migration and EMT responses and is associated with hypoxia-driven NED in PCa after ADT. Mechanistically, hypoxia enhances the MCTP1-mediated calcium/AKT pathway to stabilize SNAI1 in PCa to promote EMT and NED by increasing the SNAI1-driven expression of EMT and NE markers. MCTP1 knockdown abrogated hypoxia-enhanced EMT and NED by reducing calcium/AKT pathway-driven SNAI1 expression.

Conclusions

Our study shows the molecular mechanism by which hypoxia-associated ZBTB46/FOXA2/HIF1A transcription factor interaction upregulates the calcium sensor transmembrane protein MCTP1 in ADT-

resistant PCa, and explores how MCTP1 promotes NED and EMT in PCa by upregulating SNAI1-driven EMT and NE markers.

Background

Castration-resistant prostate cancer (PCa) (CRPC) is derived from androgen-sensitive PCa recurrence after androgen deprivation therapy (ADT) [1]. Based on the molecular features of CRPC, the treatment strategy consists of androgen receptor (AR) signaling blockers and non-specific chemotherapeutic drugs; however, persistent inhibition of AR signaling changes disease progression to a neuroendocrine (NE) phenotype known as NE PCa (NEPC) in 10–20% of CRPC cases [2–4]. These cases were identified as having more stem cell-like or AR-low features, which may express NE-specific markers such as chromogranin A (*CHGA*), γ-enolase (*ENO2*), synaptophysin (*SYP*), and N-Myc (*MYCN*), instead of AR-signaling-responsive genes (*KLK3, TMPRSS2*, and *NKX3-1*) [5, 6]. Complete loss of or lower AR signaling in NEPC leads to decreased levels of serum prostate-specific antigen (PSA), which increases the difficulty in early diagnosis [7, 8]. Prostate tumors that undergo NE differentiation (NED) are common in locally advanced or metastatic PCa after ADT, characterized by an aggressive clinical course and poor prognosis [9]. Genetic or molecular biomarkers are urgently needed to provide prognostic detection and stratified therapy for NEPC patients.

Hypoxia can induce NED, which may be a response to PCa progression induced by ADT, chemotherapy, and radiotherapy [10]. Hypoxia-inducible factor (HIF) is activated by hypoxia and regulates the expression of downstream genes by acting as a primary transcription factor [11]. ADT-induced hypoxia decreases the expression of AR and Notch signaling members Hey1 and Hes1, leading to a loss of androgen dependency [12, 13]. Several co-regulators of HIFs have been identified, such as ONECUT2/Smad3, PHF8/KDM3A, and FOXA2, which mediate HIF genomic binding to drive NE plasticity [10, 14, 15]. FOXA2 is a critical transcription factor that responds to hypoxia and is involved in endoderm formation, epithelial-to-mesenchymal transition (EMT), and NEPC development [16, 17]. Activated FOXA2 is a pioneer factor that acts as an anchor point for early transcription factors to bind to unfolded chromatin [18]. In PCa, FOXA2 is highly clinically specific as it promotes NED by reducing MASH1 [19] and increasing the expression of neurogenetic factors (HES6, SOX9, and KDM3A) [20].

Bone metastases have been reported to be associated with activated calcium transport molecular factors and signaling pathways [21]. However, the activated calcium transport signaling pathways involved in NED progression remain unclear. Using chromatin immunoprecipitation (IP) (ChIP)-sequencing (Seq), transcriptome analyses, and clinical sample validation, we identified multiple C2 domains transmembrane protein 1 (MCTP1) as a candidate biomarker of NEPC, as it may be upregulated by hypoxia-associated ZBTB46/FOXA2/HIF1A signaling in PCa after ADT. MCTP1 is a transmembrane protein with three C2 domains that strongly interacts with calcium ions [22]. Although the actual function of MCTP1 remains unclear, cumulative studies suggest that MCTP1 may be involved in the development of the neuronal system and modulation of synaptic function, including neurotransmitter release and presynaptic homeostatic plasticity through calcium sensing [23–26]. There are few studies on MCTP1 in

cancer progression, but it is known that MCTP1 may be involved in the development of drug resistance in ovarian cancer according to microarray-based detection [27], and it has been shown to be upregulated in breast cancer [28]. Here, we studied the role of MCTP1 in the relationship between hypoxia-induced EMT and NED progression in PCa. Our results demonstrated the oncogenic role of MCTP1 in PCa and estimated the effect of MCTP1 on the enhancement of EMT and NED by upregulating the calcium/AKT pathway-driven SNAI1 expression.

Methods

Cells, Constructs, and Reagents

AR-positive PCa cell lines VCaP, LNCaP, C4-2, and 22Rv1 and AR-negative PCa cell line PC3 were obtained from ATCC and cultured in RPMI-1640 medium (Thermo Fisher Scientific, 11875-085) with 5% fetal bovine serum (FBS; EMD Millipore, TMS-013-BKR). NEPC-like LASCPC01 cells were obtained from ATCC and cultured in RPMI-1640 medium composed of 10 nM hydrocortisone (Sigma-Aldrich, H0888), 1´ insulin/transferrin/selenite (Thermo Fisher Scientific, 41400-045), 200 nM β-estradiol (Sigma-Aldrich, E2758), and 5% FBS. ADT-resistant C4-2-MDVR cells were derived from C4-2 cells cultured with 20 μM enzalutamide (MDV3100; Selleckchem, S1250) for six months. All cells were tested for mycoplasma contamination using a PCR Mycoplasma Detection Kit (Omicsbio, G238) within six months before use. To mimic ADT, cells were cultured in 5% charcoal-stripped serum (CSS; Thermo Fisher, 12676-029)-containing medium under standard culture conditions for 48 h. Short-term treatment with the AR antagonist was performed with 20 μM MDV3100 for 48 h. The AR ligand was treated with 10 nM dihydrotestosterone (DHT; Selleckchem, S4757) for 24 h. For hypoxic conditions, cells were cultured in a hypoxic chamber (5% O_2) or treated with 10 μM dimethyloxallyl glycine (DMOG; Selleckchem, S7483) for 24 h. Cells with a non-target control, ZBTB46-, MCTP1-, or SNAI1-knockdown (KD) were used for luciferase (Luc), ZBTB46, MCTP1, or SNAI1 short hairpin (sh)RNA vectors (pKLO.1) obtained from RNAi Core Laboratory (Academic Sinica, Taipei, Taiwan). Cells stably expressing ZBTB46, MCTP1, and SNAI1 were generated by transfecting each cDNA-encoded or empty vector (EV) (pcDNA3.1(+) or pCDH-CMV-MCS-EF1-Puro, System Biosciences); 2×10^5 cells/six-well plate were transfected with 5 μg DNA and selected with puromycin for 1 month. Mutants of different FOXA2 fragments were constructed in the pcDNA3.1(+)/C-(K)-DYK (Flag) vector (GenScript) and transiently transfected into LNCaP cells. The pGreenFire1-ISRE lentiviral vector (System Biosciences) was used to construct a human *MCTP1* regulatory sequence containing ZBTB46, HIF1A, and FOXA2-response elements located on chromosome 5:94706192 (HRE1: -2550), 94706427 (HRE2: -2316), 94706707 (FRE1: -2037), 94707228 (FRE2: -1517), 94707384 (FRE3: -1362), 94707396 (FRE4: -1350), and 94707923 (ZRE1: -825) at GRCh38. Human *CHGA, SYP*, and *ENO2* regulatory sequence reporter plasmids containing E-boxes were respectively located on chromosome 14:93387408 (*CHGA*/E box1: -2018), 93388321 (*CHGA*/E box2: -1106), 93388458 (*CHGA*/E box3: -970), 93389496 (*CHGA*/E box4: +66), and 93389687 (*CHGA*/E box5: +256); chromosome X:49052257 (*SYP*/E box1: -2013), 49052717 (*SYP*/E box2: -1554), 49053405 (*SYP*/E box3: -867), and 49054527 (*SYP*/E box4: +253); chromosome 12: 7022136 (*ENO2*/E box1: -774), 7022373 (*ENO2*/E box2:

-538), and 7022492 (*ENO2*/E box3: -420) at GRCh37. Response element mutations were performed using the Site-Directed Mutagenesis System Kit (Invitrogen, A13282). All the primers used for these constructs are listed in Supplementary Table 1. All constructs were verified using DNA sequence analysis.

Western Blot (WB) Analysis

Cells grown in six-well plates (10^6 cells/well) were lysed in 150 µl RIPA buffer (Thermo Fisher Scientific, 89900) containing a complete protease inhibitor cocktail (Roche, 11697498001) and phosphatase inhibitors (Roche, 4906845001). Protein samples were quantified using Bradford reagent (Bio-Rad, 5000006) and separated by sodium dodecyl sulfate-polyacrylamide gel electrophoresis (SDS-PAGE). After transferring to polyvinylidene difluoride (PVDF) or nitrocellulose membranes (Thermo Fisher Scientific), the blots were blocked with 5% bovine serum albumin (BSA; Sigma-Aldrich) in PBST. Primary antibodies were incubated overnight at 4 °C, and secondary antibodies were incubated at room temperature for 1 h, as listed in Supplementary Table 2. Protein bands were visualized using enhanced chemiluminescence (ECL) plus WB detection reagents (Millipore, WBULS0100).

Reverse-Transcription (RT)-Quantitative Polymerase Chain Reaction (qPCR)

Total messenger (m)RNA was isolated using the RNeasy Midi Kit (Qiagen, 74004). For RT, 1 µg of total RNA was used with the iScript™ Complementary (c)DNA Synthesis Kit (Bio-Rad, 1708890). Amplification was performed using iTaq Universal SYBR Green Supermix (Bio-Rad, 1725120). For all primer pairs, the thermocycler was run with an initial 95 °C incubation for 10 min, followed by 40 cycles at 95 °C for 15 s and 60 °C for 1 min. All reactions were normalized to human glyceraldehyde-3-phosphate dehydrogenase (*GAPDH*) expression and run in triplicate. All the primers used for qPCR are listed in Supplementary Table 3.

IP-WB Analysis

IP-WB assay was performed using the Pierce™ classic magnetic IP/CO-IP kit (Thermo Fisher Scientific, 88804). For hypoxic treatment, 2×10^7 PC3 cells expressing ZBTB46-KD or a non-target control were treated in 10-cm dishes with 10 µM DMOG in FBS-containing medium or incubated in a hypoxic chamber (1% O_2) for 24 h. For interactions between FOXA2/ZBTB46, LNCaP cells expressing DYK-tagged FOXA2-mutants were treated with 10 µM DMOG (Selleckchem, S7483) for 24 h and lysed with IP buffer (0.025 M Tris-HCl (pH 7.4), 0.15 M NaCl, 0.001 M EDTA, 1% NP40, 5% glycerol, and 1% protease inhibitor cocktail) for 15 min on ice, followed by centrifugation at 13,000 ×*g* for 10 min at 4 °C. Subsequently, 500 µg of the protein supernatant was incubated with 2 µg DYK antibody (GenScript, A00187S) overnight at 4 °C. Protein A/G magnetic beads were then added and incubated for 1 h on a shaker at room temperature. After washing the beads thrice with IP buffer, the immune complex was collected on ice and subjected to WB analysis. The antibodies used for IP are listed in Supplementary Table 4.

Immunohistochemical (IHC) Staining

Tissue microarray (TMA) sections containing ZBTB46, FOXA2, and HIF1A from 40 patients with primary PCa were purchased from Super Bio Chips (CA4). Both of PCa TMA sections included 16 normal prostatic samples, 36 adenocarcinomas with a Gleason score of ≤6, 45 adenocarcinomas with a Gleason score of 7, and 19 adenocarcinomas with a Gleason score of ≥8, and TMA sections included 13 cases of small cell PCa (SCPC) to validate MCTP1, ZBTB46, and HIF1A were obtained from Duke University School of Medicine (Durham, NC, USA). The use of TMA at Duke University School of Medicine was approved by the Duke University School of Medicine Institutional Review Board (protocol ID: Pro00070193). The antibodies used for IHC staining are listed in Supplementary Table 5. Unstained sections were deparaffinized using a Target Antigen Retrieval Solution (DAKO, S1699) was used, and the mixture was autoclaved for 10 min for antigen retrieval. A 3% hydrogen peroxide solution was used to block endogenous peroxidases. All sections were blocked with Cyto Q Background Buffer Reagent (Innovex Biosciences, NB306). The primary antibody was diluted with Target Antigen Retrieval Solution (DAKO, S1699) and incubated overnight at 4 °C. The secondary antibody was incubated at room temperature for 30 min, and bound peroxidase was detected using an ABC Peroxidase Kit (Vector Labs, PK-6100) and DAB (DAKO, K3468). All IHC slides were counterstained with hematoxylin. For histomorphological analysis of tissue sections, microscopic images were obtained at 200´ magnification using an Axioplan microscope system (Zeiss).

ChIP Assay

The EZ Magna ChIP A kit (Sigma-Aldrich, 17-10086) was used to perform ChIP assays according to a modified protocol. In total, 10^7 parental C4-2, C4-2-MDVR, or C4-2 cells treated with 10 μM DMOG for 24 h or PC3 cells expressing the non-target control (Luc), ZBTB46-KD or MCTP1-KD shRNA vector in 10-cm dishes were cross-linked with 1% formaldehyde in culture medium at room temperature for 15 min. One milliliter of 10´ glycine was added to terminate fixation, and the cells were washed twice with cold phosphate-buffered saline (PBS) containing complete protease and phosphatase inhibitors (Roche, 11697498001 and 4906845001). The harvested cells were centrifuged at 10^4 rpm, and the cell pellet was resuspended in 0.5 ml of cell lysis buffer containing 1× Protease Inhibitor Mix II and incubated on ice for 15 min. Nuclei were collected by centrifugation at 10^4 rpm at 4 °C for 10 min and resuspended in nuclear lysis buffer. Chromatin was sonicated for 20 s using a micro-tip sonicator (Branson Sonifier 250) and then cooled on ice for 1 min. The total sonication time for each sample was 5 min. This process produced DNA fragments approximately 100–300 bp in size. The sheared chromatin was separated and immunoprecipitated with immunoglobulin G (IgG) or a primary antibody at 4 °C overnight. The ChIP antibodies and PCR primers used are listed in Supplementary Table 6. Predictions of transcription factor-binding sites in the promoter region were obtained using Alibaba 2.1 program (gene-regulation.com).

Promoter Reporter Assay

Promoter function was analyzed using fluorescence-activated cell sorting (FACS), and relative median fluorescent intensity (MFI) values of green fluorescence protein (GFP) were measured by FACS using FACSDiva software (BD Biosciences), and results were normalized to the value of the vehicle. For the

ZBTB46, FOXA2, and HIF1A-response element reporter assays, 12-well plates (5×10^4 cells/well) of C4-2 cells treated with 10 μM MDV3100, 10 μM DMOG, or vehicle control (dimethyl sulfoxide, DMSO) were transiently transfected with 1 μg *MCTP1* regulatory sequence reporter and 1 μg EV, ZBTB46, HIF1A, and FOXA2 full-length cDNA vectors. For the E-boxes-containing *CHGA, SYP,* and *ENO2* genes reporter assays, PC3 cells expressing Luc, MCTP1-KD, or SNAI1-KD shRNA vector were treated with DMSO or 10 μM DMOG for 24 h. Three independent experiments were performed in triplicates.

Proliferation Assay

LNCaP and C4-2 cells stably transfected with the EV or MCTP1 expression vector or PC3 cells stably transfected with Luc or MCTP1-KD shRNA vector were seeded at a density of 2×10^3 cells/well in 96-well plates and treated with 10 μM DMOG in FBS-containing medium for 24 h. The experiment was performed with multiple wells at each time point and the average value was determined. Every day, the cells were stained with 0.5% crystal violet for 15 min, rinsed with distilled water, and air dried. At the end of the experiment, 100 μl of 50% ethanol containing 0.1 M sodium citrate was added to each well to dissolve the crystal violet, and the absorbance was quantified at an OD 550-nm wavelength on a microplate reader.

Invasion and Migration Assay

For invasion and migration assays, LNCaP and C4-2 cells stably transfected with the EV or MCTP1 expression vector or PC3 cells stably transfected with Luc or MCTP1-KD shRNA vector combined with 10 μM DMOG treatment for 24 h were resuspended at a concentration of 3×10^3 cells/ml in serum-free medium. For the invasion assay, resuspended cells were diluted by adding 200 μl of 10-fold serum-free medium to prepare Matrigel-coated Transwell Petri dishes (Corning, 354234). The top of the Matrigel was inoculated with serum-free medium (2.5×10^5 cells/well). The lower chamber was filled with 600 μl of serum-containing medium. After 12 h, cells that had invaded the Matrigel-coated Transwell were fixed and stained with 0.5% crystal violet for 15 min. A phase-contrast microscope (Olympus) was used to capture a snapshot of the invading cells under the membrane and three replicates were counted each time. The migration assay was performed using transwells without Matrigel, and the cells were fixed and stained, as described for the invasion assay.

Tumorigenicity Assays in Mice

The protocol for the *in vivo* tumorigenicity assay was based on *Guidelines for Care and Use of Laboratory Animals* from the Council of Agriculture, Executive Yuan, Taiwan and was approved by the Taipei Medical University Institutional Animal Care and Use Committee (approval ID: LAC-2021-0481). Six-week-old CAnN.Cg-*Foxn1*^{nu}/CrlNarl mice were purchased from the National Laboratory Animal Center (NLAC, Taipei, Taiwan). Mice were randomized into three groups and subcutaneously injected with 2×10^6 cells/site (suspended in 100 μL of a mixture of Matrigel matrix and culture medium) of PC3 cells stably transfected with control Luc or MCTP1-KD shRNA vectors on the right side of the flank under double-blind conditions. The tumor diameter was monitored once a week, and mouse weight was monitored for 7

weeks. The mice were euthanized by CO_2 anesthetization, and the tumors were collected, weighed, paraffin-embedded, and sliced for subsequent IHC staining. The tumor diameter was converted into volume according to the following formula [29]: ; where V, H, W, and L are the volume, height, width, and length, respectively.

Measurement of Intracellular-free Calcium

PC3 cells were stably transfected with Luc or MCTP1-KD shRNA vector and treated with 10 μM DMOG in calcium-free Hank's balanced salt solution (HBSS; Invitrogen, 14170161) for 24 h. The cells were washed with HBSS and pre-incubated with 5 μM Fluo 8-AM (Abcam, ab142773) at 37 °C for 60 min. After washing, cells were cultured in calcium-free HBSS at 37 °C for 30 min. Fluorescence signals were captured using a fluorescence microscope (Olympus IX73). The relative mean intensity of Fluo 8-AM was measured by FACS (BD Biosciences) using FACSDiva software (BD Biosciences) and normalized to the value of the vehicle. Three independent experiments were performed in triplicates.

Statistical Analysis

All data are presented as mean ± standard error of the mean (SEM). Statistical calculations were performed using GraphPad Prism V8.0 (GraphPad Software). Differences between individual groups were determined using Student's *t*-test or one-way analysis of variance (ANOVA), followed by Bonferroni's post-test for comparisons among three or more groups. Correlations between IHC staining results of relative intensity of ZBTB46, FOXA2, and HIF1A was determined by correlation XY analyses using GraphPad Prism. For tumor grade association analysis of IHC staining of the primary PCa TMA collected from Duke University School of Medicine, *p* values were calculated using a Chi-squared test performed with SPSS statistical software ver. 18.0 (IBM SPSS). A log-rank test was used for the survival curve analysis of 111 PCa patients (98 primary and 13 metastatic samples), and the hazard ratios of MCTP1 high (*n*=56)/MCTP1 low (*n*=55) were determined for each group. The method for determining the cut-off values was predetermined by half the number of patients.

Results

ZBTB46 upregulation is associated with HIF1A/FOXA2 signaling in PCa after ADT

We sought to determine the signaling profile that characterizes the progression of ADT-resistant PCa. Total mRNA was prepared from androgen-dependent LNCaP cells cultured for six months with the AR antagonist enzalutamide (MDV3100), and RNA-Seq analysis was used to determine the signaling pathway upregulated after androgen deprivation. We found that the HIF1 signaling pathway was significantly upregulated in cells exhibiting ADT resistance (Supplementary Fig. 1A). Our previous report showed that ZBTB46 was overexpressed in PCa cells after the development of ADT resistance [30-32]. To evaluate whether the abundance of ZBTB46 was associated with HIF1A in PCa cells after ADT, we verified the expression of ZBTB46, HIF1A, and the HIF1A cofactor FOXA2 in AR-positive LNCaP cells in response to ADT. We found that cells treated with CSS-containing medium (to mimic ADT) showed

increased ZBTB46 expression, which was positively correlated with HIF1A and FOXA2, and negatively correlated with the expression of androgen-responsive marker (NKX3-1) (Fig. 1A). Moreover, increased ZBTB46 expression was associated with the upregulation of HIF1A and FOXA2 as well as hypoxia target markers of FOXA2 (HES6, SOX9, and KDM3A) in CSS-treated LNCaP cells (Fig. 1B). However, CSS-treated cells rescued with the AR ligand DHT showed a decrease in ZBTB46, HIF1A, FOXA2, HES6, SOX9, and KDM3A and an increase in androgen-responsive markers (NKX3-1 and KLK3) (Fig. 1B). These results suggest that inactivation of the AR pathway may be involved in ZBTB46 upregulation, which is associated with hypoxia-induced HIF1A/FOXA2 signaling. Increased ZBTB46 expression was confirmed in MDV3100-resistant C4-2 cells, and was related to the upregulation of HIF1A, FOXA2, HES6, SOX9, and KDM3A (Fig. 1C). Interestingly, ZBTB46 upregulation was observed in various PCa cell lines under hypoxic conditions (Fig. 1D). Furthermore, a dose-dependent increase in ZBTB46 protein was correlated with HIF1A and FOXA2 proteins in AR-negative PC3 cells treated with the hypoxia activator DMOG (Fig. 1E), and increased ZBTB46 expression was correlated with the induction of HIF1A and FOXA2 in AR-positive C4-2 and LNCaP cells cultured in hypoxic incubators (Fig. 1F). In DMOG-treated PC3 and LNCaP cells, elevated mRNA levels of ZBTB46 were correlated with the upregulation of HIF1A, FOXA2, HES6, SOX9, and KDM3A (Fig. 1G, H). These results suggested that the increase in ZBTB46 expression in PCa may be related to the activation of HIF1A/FOXA2 signaling under hypoxic conditions. To study the relationship between ZBTB46 and FOXA2 or HIF1A in clinical tissue samples, we analyzed a PCa TMA (Super Bio Chips, CA4) comprising of 40 cases of primary PCa. The IHC results showed a positive correlation between ZBTB46 and FOXA2 or HIF1A in consecutive tissue sections of prostate tumor samples (Fig. 1I, J). We analyzed the relationship between ZBTB46 and hypoxia pathways in The Cancer Genome Atlas (TCGA) PCa dataset using gene set enrichment analysis (GSEA) and found that patients with upregulated ZBTB46 were robustly associated with enhanced hypoxic response signatures (Fig. 1K). In addition, we found that upregulation of ZBTB46 was positively correlated with the gene signature response to hypoxic targets of HIF1A and FOXA2, as confirmed by GSEA in TCGA PCa database (Supplementary Fig. 1B), and high mean expression levels of ZBTB46 were significantly positive associated with HIF1A and FOXA2 in the Taylor PCa dataset (GSE21036; Supplementary Fig. 1C). These results suggest that ADT may induce the accumulation of ZBTB46 and that the upregulation of ZBTB46 may be associated with hypoxia-associated HIF1A/FOXA2 signaling in PCa.

ZBTB46 interacts with the HIF1A/FOXA2 complex

To study whether ZBTB46 is a potential hypoxia-associated transcription factor that interacts with FOXA2 and HIF1A, we performed IP-WB through IP of ZBTB46 and immunoblotted ZBTB46, FOXA2, and HIF1A proteins in PC3 cells under hypoxic conditions. Compared with the vehicle control, stable interactions between ZBTB46 and FOXA2 or HIF1A proteins were observed in cells treated with DMOG or hypoxia chamber (Fig. 2A). We also found an increased interaction between FOXA2 and ZBTB46 or HIF1A under hypoxic conditions through IP of FOXA2 and immunoblotted of the same proteins (Fig. 2B), suggesting that ZBTB46 physically interacts with the HIF1A/FOXA2 complex. Conversely, decreased interactions among ZBTB46, FOXA2, and HIF1A were observed in ZBTB46-KD cells, even in DMOG-treated cells (Fig. 2C). In addition, increased expression of ZBTB46, FOXA2, HIF1A, and hypoxia target markers of FOXA2

(HES6 and SOX9) was observed in PC3 cells treated with DMOG or hypoxia chamber, whereas decreased expression of HES6 and SOX9 was observed in cells transfected with ZBTB46-KD, regardless of hypoxic conditions (Fig. 2D, E). These observations suggested that ZBTB46 may regulate the expression of hypoxia/FOXA2-responsive genes. To map the FOXA2 domains critical for its interaction with ZBTB46 under hypoxia, we constructed a series of FOXA2 protein mutants with DYK-tagged FLAG (Fig. 2F), which further validated the interaction between ZBTB46 and FOXA2 under hypoxic conditions. AR-positive LNCaP cells were co-transfected with wild-type (WT) ZBTB46 cDNA and DYK-tagged FOXA2 mutants and treated with DMOG. The results showed that the full-length FOXA2 and FOXA2_361 mutant had increased interactions with ZBTB46 in cells treated with DMOG compared to the FOXA2_252 or FOXA2_113 mutants (Fig. 2G). This suggests that domains 252-361 of FOXA2 are the core interacting domains that bind ZBTB46 under hypoxic conditions. We also found upregulation of hypoxia/FOXA2 response markers (HES6 and SOX9) in cells transfected with full-length FOXA2 or the FOXA2_361 mutant compared to FOXA2_252 or FOXA2_113 mutants (Fig. 2H-I). Notably, increased HES6 and SOX9 expression was found in full-length FOXA2 or the FOXA2_361 mutant transfected cells treated with hypoxic conditions (Fig. 2H, I) or co-transfected with the ZBTB46 expression vector (Fig. 2J). These data suggest that ZBTB46 may be a co-activator of the hypoxia-related FOXA2 transcription factor, which interacts with domains 252-361 of FOXA2 and promotes hypoxia/FOXA2-related signaling in PCa cells.

MCTP1 is a candidate target of ZBTB46/FOXA2/HIF1A regulatory signaling

Next, we analyzed ZBTB46 and HIF1A expression with gene signatures that reflect FOXA2-targeted responsive genes in TCGA PCa dataset using GSEA to investigate the downstream targets of hypoxia-related ZBTB46/FOXA2/HIF1A regulatory signaling. We found that tissues expressing high levels of ZBTB46 and HIF1A were positively associated with gene signatures of upregulated FOXA2-targeted responsiveness [33] (Supplementary Fig. 2A, B). *MCTP1* was present at the top of the gene list of ranked metric scores in both GSEAs, based on the significance of the false discovery rate (FDR) and *p* value in both assays (Supplementary Fig. 2A, B). To investigate whether MCTP1 stimulation might be upregulated by hypoxia-related signaling in PCa, GSEA was validated against hypoxia-related gene signatures in TCGA PCa dataset. The results showed that tissues expressing high levels of MCTP1 were positively associated with genes activated in response to multiple hypoxia signaling pathways (Supplementary Fig. 2C). Mean expression correlation was confirmed in TCGA PCa database, which showed that the mRNA level of MCTP1 was positively correlated with HIF1A (Supplementary Fig. 2D). Although significant MCTP1 expression has been reported in neuronal systems [23, 24, 26, 34], little is known about the regulatory mechanisms of *MCTP1* gene expression. To examine whether ZBTB46 is associated with the FOXA2/HIF1A complex and increases MCTP1 expression, we overexpressed full-length ZBTB46, FOXA2, and HIF1A cDNA vectors in AR-positive LNCaP and C4-2 cells. The results showed that overexpression of ZBTB46 caused partial increases in MCTP1 mRNA and protein levels, whereas co-transfection with FOXA2 and HIF1A significantly increased MCTP1 expression (Fig. 3A, B). We also found that co-transfection with FOXA2 and HIF1A synergistically increased ZBTB46 expression (Fig. 3A, B), suggesting a possible feedback loop for the upregulation of ZBTB46 by the FOXA2/HIF1A complex or MCTP1. To study the regulatory network between *MCTP1* and the hypoxia-FOXA2/HIF1A axis, we investigated the

binding of HIF1A/B and FOXA2 to *MCTP1* using ChIP-Seq analysis. We found a possible consensus HIF1A/B and FOXA2 elements of the *MCTP1* regulatory sequence located around chromosome 5:94600000-94650000, with potential nuclear HIF1A/B and FOXA2 binding (Supplementary Fig. 2E). We searched for sequences resembling HIF1A/B and FOXA2 response elements (HRE and FRE) in the putative *MCTP1* regulatory sequence region, and identified candidate response elements for nuclear HIF1A/B and FOXA2 in the promoter region relative to the *MCTP1* transcriptional start site (Fig. 3C). Notably, we also found a ZBTB46 response element (ZRE) in the promoter region of *MCTP1* (Fig. 3C). To determine whether ZBTB46/FOXA2/HIF1A directly binds to *MCTP1*, we performed ChIP assays and used qPCR to determine the amount of *MCTP1* DNA precipitated by ZBTB46, FOXA2, and HIF1A antibodies in the nuclear extracts of C4-2 cells in the presence of DMOG stimulation. We found that HIF1A, FOXA2, and ZBTB46 binding at the HRE1, FRE1, FRE3, FRE4, and ZRE sites significantly increased after the treatment of cells with DMOG (Fig. 3D). Consistently, increased HIF1A, FOXA2, and ZBTB46 binding was found at the same sites in MDV3100-resistant C4-2 cells compared to that in parental cells (Fig. 3E). In contrast, ZBTB46-KD reduced binding signals of HIF1A, FOXA2, and ZBTB46 in PC3 cells compared to non-target control shRNA (Fig. 3F), consistent with our hypothesis that ZBTB46 may be a core-bound transcription factor that increases FOXA2/HIF1A-mediated transcriptional activation of *MCTP1*. In addition, we performed reporter assays using DNA constructs containing single HRE, FRE, or ZRE mutations in *MCTP1* regulatory sequence cloned into a GFP reporter plasmid (Fig. 3C). DMOG-treated C4-2 cells showed significantly increased reporter gene activity in the WT reporter relative to untreated cells, whereas reduced reporter activity was observed in mutants at the HRE1, FRE1, FRE3, FRE4, and ZRE sites compared to the WT reporter, regardless of whether the cells were treated with DMOG (Fig. 3G). Similarly, increased WT reporter activity was detected in C4-2-MDVR cells, and the HRE1, FRE1, FRE3, FRE4, and ZRE sites mutants reduced reporter activity (Fig. 3H). Furthermore, the HRE1, FRE1, FRE3, FRE4, and ZRE sites mutants also disrupted the ability of HIF1A, FOXA2, and ZBTB46 cDNA vectors to induce reporter activity compared to other sites in promoter assays (Fig. 3I). These data are consistent with the mechanism by which ZBTB46, FOXA2, and HIF1A promote *MCTP1* transcription via direct physical interactions with the *MCTP1* regulatory sequence.

MCTP1 is upregulated in high-grade PCa and NEPC tumors

To study the clinical relevance of MCTP1 and the ZBTB46/FOXA2/HIF1A complex, we analyzed 16 normal prostatic samples, 36 adenocarcinomas with a Gleason score of ≤6, 45 adenocarcinomas with a Gleason score of 7, and 19 adenocarcinomas with a Gleason score of ≥8 from a PCa TMA collected from the Duke University School of Medicine (Durham, NC, USA). IHC analyses showed that cytoplasmic MCTP1, which is associated with nuclear ZBTB46, FOXA2, and HIF1A, was more abundant in high-grade tumors (Fig. 4A, B). Mean expression correlations were analyzed in TCGA PCa database, which showed that MCTP1 was positively correlated with ZBTB46 and FOXA2 (Fig. 4C). Moreover, patients whose prostate tumors showed high MCTP1 mRNA expression levels exhibited high metastatic potential, as validated in the Taylor PCa dataset (GSE21036; Fig. 4D). Furthermore, PCa patients with high MCTP1 mRNA expression exhibited shorter survival times (Fig. 4E), and these tumors were significantly associated with low prostate-specific antigen (PSA) levels in the Taylor clinical PCa dataset (Fig. 4F). We

investigated the association of MCTP1 with NEPC reprogramming-related gene signatures, as validated in TCGA PCa database by GSEA, and found that upregulation of MCTP1 was positively associated with gene signatures in response to RB1 loss of function [35], p53 mutations [36], PCa progression (KEGG, Tomlines [37], and Ouyang [38]), cell migration (Wu [39]), metastasis (Cromer [40] and Sung [41]), SCLC progression (KEGG), and NEPC differentiation (Li [42] and Beltran [42]) (Fig. 4G). We also found that increased MCTP1 expression was inversely associated with upregulation of androgen-responsive gene signatures (Fig. 4H). IHC analysis confirmed that MCTP1 was robustly increased in SCPC TMA collected from the Duke University School of Medicine (Durham, NC, USA), and a correlation analysis revealed that MCTP1 was significantly abundant in ZBTB46, FOXA2, and HIF1A-positive SCPC samples (Fig. 4I, J). These results support the association between amplification of MCTP1 and ZBTB46/FOXA2/HIF1A complex, and are related to the aggressiveness of PCa and NEPC differentiation.

Overexpression of MCTP1 is associated with ADT-induced NED of PCa

We verified the expression of MCTP1 in various PCa cell lines and found that MCTP1 was upregulated in AR-negative PC3 and NEPC-like LASCPC01 cells compared to that in AR-positive VCaP, LNCaP, C4-2, and 22Rv1 cells (Fig. 5A). Interestingly, various PCa cells treated with DMOG showed increased MCTP1 expression (Fig. 5B), and the induced protein levels of MCTP1 in AR-positive cells were associated with increased HIF1A and NE marker (CHGA and ENO2) expression in AR-positive C4-2 and LNCaP cells under hypoxic conditions (Fig. 5C). AR-negative PC3 cells treated with DMOG showed a dose-dependent increase in MCTP1 expression, which was associated with an increase in HIF1A and NE marker expression (Fig. 5D). We also found that MCTP1 overexpression in C4-2 and LNCaP cells increased mRNA and protein levels of NE markers (Fig. 5E, F). However, MCTP1-KD exhibited a decrease in NE marker levels in PC3 cells (Fig. 5G). Importantly, MCTP1-KD in PC3 cells abolished the DMOG-driven increase in NE marker levels (Fig. 5H, I). As the incidence of NEPC frequently increases following treatment with AR antagonists [43], we sought to determine the effect of ADT on MCTP1 expression. We examined the mean expression values of MCTP1 in the mRNA expression profile of LNCaP cells cultured for 11 months of androgen deprivation. Results showed that MCTP1 expression was significantly increased in cells after ADT (GDS3358; Supplementary Fig. 3A). We treated AR-positive LNCaP and C4-2 cells with MDV3100 for 1–5 months, and the results showed that MDV3100-treated cells exhibited a dramatic induction of MCTP1 compared to parental cells (Supplementary Fig. 3B). Significantly, LNCaP and C4-2 cells treated with CSS-containing medium to mimic ADT showed increased MCTP1 and NE markers, while the reduction in MCTP1 was associated with NE markers in cells in the presence of DHT (Fig. 5J and Supplementary Fig. 3C, D). Importantly, increased MCTP1 expression was associated with upregulated NE marker expression in ADT-treated cells, whereas MCTP1-KD abolished ADT-driven MCTP1 and NE marker expression (Fig. 5K, L). MCTP1 protein levels were validated in long-term MDV3100-treated cells, and we found that increased MCTP1 expression correlated with NE markers induced in MDV3100-resistant C4-2 cells (Fig. 5M, N). Conversely, decreased NE markers were found in MDV3100-resistant C4-2 cells expressing MCTP1-KD (Fig. 5M, N). Moreover, tissues expressing high levels of MCTP1 were positively associated with upregulated neurodevelopment gene signatures, as analyzed by GSEA in TCGA PCa datasets, according to the significant FDR and *p* value (Supplementary Fig. 3E).

These data suggest that hypoxia-induced MCTP1 expression may be upregulated in cells undergoing ADT resistance, and is associated with NED in PCa cells.

MCTP1 promotes cell migration and enhances SNAI1 expression

Although MCTP1 has been shown to be involved in regulating the endocytic cycle in CNS or neuronal cell synapses [23, 24, 26, 34], the functional role of MCTP1 in NED progression of PCa remains unknown. We sought to determine the role of MCTP1 in affecting the invasiveness of AR-positive LNCaP and C4-2 cells and found that MCTP1-overexpressing cells exhibited enhanced cell migration and invasion (Fig. 6A, B). We further examined the functional relevance of MCTP1-mediated cell proliferation in the same two cell lines and found that cells with ectopic MCTP1 expression exhibited increased proliferation compared with EV-bearing cells (Fig. 6C). Moreover, migration and invasiveness of AR-negative PC3 cells were significantly increased when cells were treated with DMOG, whereas these effects were decreased in MCTP1-KD cells, regardless of DMOG treatment (Fig. 6D). Furthermore, the treatment of cells with DMOG increased cell proliferation, whereas MCTP1-KD reduced the effects of DMOG-driven cell proliferation (Fig. 6E). As therapy-induced NEPC is highly associated with EMT phenotypes [44], we examined associations between MCTP1 levels and EMT-related gene signatures in TCGA PCa dataset using GSEA. We found that high MCTP1 levels were positively associated with the upregulation of EMT-related gene signatures (Supplementary Fig. 4A). Next, we analyzed the levels of EMT-associated transcription factors in cells overexpressing MCTP1. Results showed that cells overexpressing MCTP1 exhibited significantly upregulated mRNA and protein levels of SNAI1 and a slight increase in TWIST1 compared with other EMT-associated transcription factors (Fig. 6F and Supplementary Fig. 4B, C). Conversely, protein levels of SNAI1 were significantly reduced in PC3 cells expressing MCTP1-KD compared to other transcription factors (Fig. 6G). We hypothesized that the stimulation of SNAI1 might be associated with hypoxia-induced MCTP1 expression in PCa cells. The results showed that MCTP1 associated with SNAI1 was increased in DMOG-treated PC3 cells compared to untreated cells; however, MCTP1-KD cells showed a marked decrease in SNAI1 expression, even in cells treated with DMOG (Fig. 6H and Supplementary Fig. 4D). Next, we found that PC3 cells bearing MCTP1-KD subcutaneous tumors had significantly reduced tumor growth and weight compared with mice injected with non-target control PC3 cells (Fig. 6I-K). Tumors were harvested and examined for MCTP1, SNAI1, NE, proliferation (KI67), and hypoxia (CA9) markers by IHC. The results showed that tumors derived from PC3 cells with MCTP1-KD had reduced SNAI1 expression compared with control tumors, which was associated with reductions in ENO2, KI67, and CA9 (Fig. 6L, M). These data suggest that SNAI1 overexpression may be associated with MCTP1-driven EMT and NED progression in PCa under hypoxia.

MCTP1 promotes the NED and EMT process in PCa cells by activation of the calcium-driven PI3K/AKT/SNAI1 signaling

Recent studies have demonstrated that calcium-related signaling, such as the PI3K/AKT pathway, regulates EMT during cancer progression [45]. Activation of the PI3K/AKT pathway downregulates GSK-3β, thereby stabilizing SNAI1 and leading to SNAI1 entering the nucleus and promoting the expression of

EMT-related factors [46]. However, high levels of intracellular calcium driven by MCTP1 promote EMT and NED processes in PCa remain unknown. We explored the role of MCTP1 in regulating intracellular calcium levels in PCa, affecting PI3K/AKT signaling, and its role in regulating SNAI1-driven EMT and NED processes. IF staining using the green fluorescent calcium binding dye Fluo-8 AM showed that PC3 cells expressed high levels of intracellular calcium under hypoxic conditions, whereas cells expressing MCTP1-KD reduced intracellular calcium levels, regardless of DMOG treatment (Fig. 7A). Similarly, flow cytometry analysis showed that DMOG treatment increased the intensity of the fluorescence signal in PC3 cells; however, the fluorescence signal was decreased in cells expressing MCTP1-KD (Fig. 7B). Notably, dose-dependent DMOG treatment increased levels of MCTP1, AKT phosphorylation, and SNAI1 in C4-2 cells (Fig. 7C). Conversely, cells expressing MCTP1-KD showed reduced levels of MCTP1, AKT phosphorylation, and SNAI1, even in cells treated with DMOG (Fig. 7D). These data suggest that MCTP1 activation may be involved in PI3K/AKT signaling-mediated SNAI1 expression in PCa cells under hypoxia. We focused on the SNAI1-mediated signaling component of gene regulation driven by MCTP1, through which it regulates the expression of NEPC-associated gene. We searched for sequences resembling the putative E-box in the *CHGA, SYP,* and *ENO2* regulatory sequence regions. Interestingly, we identified five, four, and three putative E-boxes in the *CHGA*, *SYP,* and *ENO2* regulatory sequences, respectively (Fig. 7E). ChIP assays were performed by IP of nuclear SNAI1 using SNAI1 antibody from nuclear extracts of PC3 cells expressing control or MCTP1-KD, following treatment with DMOG. Significantly, increased nuclear SNAI1 binding at the putative E-box of the *CHGA* (E-boxes 2, 3, and 5), *SYP* (E-boxes 2 and 3), and *ENO2* (E-boxes 2 and 3) genes was found in DMOG-treated PC3 cells, whereas the binding signals were decreased in cells expressing MCTP1-KD, regardless of DMOG treatment (Fig. 7F-H). In addition, reporter assays were performed using a DNA construct containing wild-type E-boxes from the *CHGA*, *SYP,* and *ENO2* regulatory sequences cloned into a GFP reporter plasmid (Fig. 7E). Induction of reporter activity was observed in PC3 cells treated with DMOG; however, DMOG-treated cells expressing MCTP1-KD showed significantly decreased reporter activity of *CHGA*, *SYP,* and *ENO2* relative to untreated cells (Fig. 7I). Similarly, we found that *CHGA, SYP* and *ENO2* gene reporter activities were reduced in PC3 cells expressing SNAI1-KD, regardless of DMOG treatment (Fig. 7J). We also found that the induction of SNAI1 was associated with increased mRNA levels of NE (CHGA, SYP, and ENO2) and EMT (CD44 and VIM) markers in cells after SNAI1 cDNA overexpression (Supplementary Fig. 4E, F). Moreover, increases in SNAI1, NE, and EMT markers were observed in cells treated with DMOG, and a significant decrease was found in cells transfected with SNAI1-KD (Fig. 7K). These data suggest that MCTP1 activation may be involved in SNAI1-mediated NE and EMT marker expression in PCa cells under hypoxic conditions. In summary, our study shows that ADT-induced ZBTB46/FOXA2/HIF1A-driven MCTP1 promotes EMT properties associated with NED progression in PCa cells by upregulating MCTP1/SNAI1, mediated by the calcium-related PI3K/AKT signaling pathway (Fig. 7L).

Discussion

In this study, we sought to understand the effects of MCTP1 on the progression of NED in ADT-resistant PCa. MCTP1 is a calcium-sensing protein that contains three calcium-binding C2 domains [22]. Calcium

sensing is known to promote cell proliferation in androgen-dependent or independent PCa [47, 48]. Our results demonstrated that MCTP1 was the most abundant gene that was significantly upregulated in ZBTB46 and HIF1A-high tissues among the hypoxia target markers of FOXA2. We showed a direct interaction between the FOXA2/HIF1A complex and the ADT-induced transcription factor ZBTB46, and demonstrated that MCTP1 upregulation is mediated by the ZBTB46/FOXA2/HIF1A complex, providing evidence for its role in MCTP1 in cellular function leading to androgen-independent PCa or NEPC development. Our data support FOXA2 upregulation as an activator of HIF1A-driven NEPC differentiation [16, 17]. A study on mouse neurons indicated that MCTP1 mediates transferrin uptake in presynaptic axons, suggesting a crucial role for MCTP1 in neuronal development [26]. In addition, MCTP1 regulates neurotransmitter release in *Caenorhabditis elegans* [23] and is involved in neuronal cell secretion of peptide hormones [26]. Although MCTP1 has been implicated in various neuropsychiatric diseases and is involved in drug resistance in ovarian and esophageal cancers [27, 49], we demonstrated that *MCTP1* is regulated by hypoxia-associated ZBTB46/FOXA2/HIF1A transcription factors, which mediate malignant progression and contribute to SNAI1-driven NED and EMT in PCa.

FOXA2 was shown to interact with hypoxia-HIF1A signaling to promote NEPC progression [50], and our results demonstrated that the HIF1A/FOXA2 complex interacts with ZBTB46 to upregulate MCTP1 expression in PCa cells after ADT. MCTP1 was strongly upregulated in cells subjected to either ADT or hypoxia, whereas this stimulation was abolished in cells with ZBTB46-KD, suggesting that MCTP1 is upregulated by ZBTB46 after AR signaling inhibition. ADT induces hypoxia in PCa cells by upregulating HIF1A [51, 52]; however, the mechanisms underlying HIF1A upregulation due to loss of AR function after ADT and further activation of NED remain unknown. Since our recent studies uncovered a potential regulatory network in which ZBTB46 is upregulated in PCa following ADT [30–32], our current results link the inhibition of AR signaling-driven NED to hypoxia signaling through ZBTB46/FOXA2/HIF1A complex upregulation. We further demonstrated that ZBTB46 cooperates with HIF1A/FOXA2 to mediate MCTP1 expression, resulting in calcium-related signaling pathways that drive NED and EMT in ADT-resistant PCa.

MCTP1 may affect calcium ion channel transport, thereby mediating the interaction between tumor cells and the tumor microenvironment [53, 54]. We observed an abundance of MCTP1 in patients with high-grade PCa and NEPC. However, it remains unclear whether MCTP1 drives NED in PCa tumors by activating calcium ion channel transport. Calcium sensing is also involved in neural differentiation [55]. MCTP1 is a calcium sensor that contains three calcium-binding C2 domains [56], is involved in endocytosis, and regulates oxidative stress and reactive oxygen species (ROS) production in neuronal cells [26]. Increased SNAI1 protein levels have been found to be involved in the upregulation of ion channel transport in response to TGF-β signaling [57, 58] and correlated with the NEPC phenotype [59]. Our results showed that activation of MCTP1 may promote the PI3K/AKT signaling-driven stimulation of SNAI1 to upregulate NE and EMT marker expression in PCa cells under hypoxic conditions. We studied the molecular mechanism of the interaction between calcium-related signaling and androgen-independent pathways and explored how MCTP1 promotes EMT and the development of NEPC by activating SNAI1-driven NE and EMT marker upregulation.

Our previous studies revealed a model for the ADT-induced ZBTB46 transcription factor driving NED [30–32]. Here, we further discovered that upregulation of ZBTB46 might be linked to hypoxia, indicating that ZBTB46 interacts with the hypoxia-HIF1A/FOXA2 pathway, leading to the activation of the calcium sensor transmembrane protein MCTP1. Our study contributes to the knowledge of the oncogenic function of MCTP1 in NEPC development and its upregulation by ZBTB46/FOXA2/HIF1A signaling. We observed that upregulation of MCTP1 may promote NED in PCa cells and is involved in the increase in EMT and cell motility. For clinical applications, our findings will help assess whether MCTP1 could be used as a biomarker for the diagnosis of NEPC and as a therapeutic target. Conventional regimens for NEPC include taxanes and platinum-based chemotherapeutic drugs, which frequently induce severe adverse effects [60]. Therefore, MCTP1 inhibition may prevent malignant transformation or NEPC development in PCa after ADT. We hypothesized that strategies targeting MCTP1 may be effective against androgen-independent PCa by modulating EMT and NED responses, which in turn determine the aggressiveness of PCa. The current lack of understanding of the mechanisms underlying NEPC development makes treatment more difficult. In addition to supporting the molecular basis of ADT-induced MCTP1 expression leading to NED and aggressiveness of PCa, our study also provides a new possibility for the clinical prognosis and treatment of NEPC.

Conclusions

We investigated the molecular mechanism by which the ADT-induced ZBTB46 transcription factor interacts with hypoxia-associated FOXA2/HIF1A transcription factors to upregulate the calcium sensor transmembrane protein MCTP1 in PCa undergoing ADT resistance and explored how MCTP1 promotes EMT and the development of NEPC by activating calcium-related signaling to enhance SNAI1-driven NE and EMT marker upregulation.

Abbreviations

ADT
androgen deprivation therapy
ChIP
chromatin immunoprecipitation
CSS
charcoal-stripped serum
CRPC
castration-resistant prostate cancer
EMT
epithelial-to-mesenchymal transition
FOXA2
forkhead box protein A2
GSEA

gene set enrichment analysis
HIF
hypoxia-inducible factor
NED
neuroendocrine differentiation
NEPC
neuroendocrine prostate cancer
MCTP1
multiple C2 domains transmembrane protein 1
PCa
prostate cancer
PSA
prostate-specific antigen
SCPC
small cell prostate cancer
TCGA
The Cancer Genome Atlas
TMA
tissue microarray
ZBTB46
zinc finger and BTB domain containing 46

Declarations

Ethics approval and consent to participate

The use of TMA at Duke University School of Medicine was approved by the Duke University School of Medicine Institutional Review Board (protocol ID: Pro00070193).

The protocol for the *in vivo* tumorigenicity assay was based on *Guidelines for Care and Use of Laboratory Animals* from the Council of Agriculture, Executive Yuan, Taiwan and was approved by the Taipei Medical University Institutional Animal Care and Use Committee (approval ID: LAC-2021-0481).

Consent for publication

Not applicable

Availability of data and material

The human clinical datasets utilized in the study are included in Additional file 1; Supplementary Methods sections

Competing interests

The authors declare that they have no competing interests.

Funding

This work was jointly supported by grants from the Ministry of Science and Technology, Taiwan (MOST109-2326-B-038-001-MY3 and MOST110-2622-B-038-002 to Y.N.L.), National Health Research Institutes, Taiwan (NHRI-EX111-11109BI to Y.N.L.), Wan Fang Hospital (110-wf-f-2 to Y.C.W.), and the Center of Excellence for Cancer Research, Ministry of Health and Welfare, Taiwan (MOHW111-TDU-B-221-014002 to Y.N.L.).

Authors' contributions

Y.C.W. and Y.N.L. designed experiments and supervised the study. W.Y.C., H.L.Y., W.H.C., K.C.J., H.R.L., V.T.N.T., P.V.T.D., and Z.Q.C. performed experiments. Y.C.W., W.Y.C., and J.H. provided human PCa samples. W.Y.C. performed histomorphometric analysis. H.L.Y. constructed the databases and performed statistical and computational analyses. M.H. assisted with animal experiments. Y.C.W. and Y.N.L. wrote, reviewed, and revised the manuscript. All authors analysed and interpreted the data.

Acknowledgements

We thank Dr. Hsing-Jien Kung (Academician of the Academia Sinica, Chair Professor of Taipei Medical University) for reading the manuscript, providing comments, and helpful suggestions.

References

1. Wade CA, Kyprianou N: **Profiling Prostate Cancer Therapeutic Resistance**. Int J Mol Sci 2018, **19**:904.
2. Teo MY, Rathkopf DE, Kantoff P: **Treatment of Advanced Prostate Cancer**. Annu Rev Med 2019, **70**:479–499.
3. Ritch C, Cookson M: **Recent trends in the management of advanced prostate cancer**. F1000Res 2018, **7**.
4. Litwin MS, Tan HJ: **The Diagnosis and Treatment of Prostate Cancer: A Review**. Jama 2017, **317**:2532–2542.
5. Vellky JE, Ricke WA: **Development and prevalence of castration-resistant prostate cancer subtypes**. Neoplasia 2020, **22**:566–575.
6. Rupniak NMJ, Katofiasc M, Burgard EC, Thor KB: **Colorectal and cardiovascular effects of [Lys(5),MeLeu(9),Nle(10)]-NKA(4–10) in anesthetized macaques**. Naunyn Schmiedebergs Arch Pharmacol 2018, **391**:907–914.
7. Vlachostergios PJ, Puca L, Beltran H: **Emerging Variants of Castration-Resistant Prostate Cancer**. Curr Oncol Rep 2017, **19**:32.
8. Apostolidis L, Nientiedt C, Winkler EC, Berger AK, Kratochwil C, Kaiser A, Becker AS, Jager D, Hohenfellner M, Huttenbrink C, et al: **Clinical characteristics, treatment outcomes and potential novel**

therapeutic options for patients with neuroendocrine carcinoma of the prostate. Oncotarget 2019, **10**:17–29.

9. Klimstra DS, Beltran H, Lilenbaum R, Bergsland E: **The spectrum of neuroendocrine tumors: histologic classification, unique features and areas of overlap**. Am Soc Clin Oncol Educ Book 2015:92–103.
10. Guo H, Ci X, Ahmed M, Hua JT, Soares F, Lin D, Puca L, Vosoughi A, Xue H, Li E, et al: **ONECUT2 is a driver of neuroendocrine prostate cancer**. Nat Commun 2019, **10**:278.
11. Semenza GL: **Hypoxia-inducible factors in physiology and medicine**. Cell 2012, **148**:399–408.
12. Geng H, Xue C, Mendonca J, Sun XX, Liu Q, Reardon PN, Chen Y, Qian K, Hua V, Chen A, et al: **Interplay between hypoxia and androgen controls a metabolic switch conferring resistance to androgen/AR-targeted therapy**. Nat Commun 2018, **9**:4972.
13. Danza G, Di Serio C, Rosati F, Lonetto G, Sturli N, Kacer D, Pennella A, Ventimiglia G, Barucci R, Piscazzi A, et al: **Notch signaling modulates hypoxia-induced neuroendocrine differentiation of human prostate cancer cells**. Mol Cancer Res 2012, **10**:230–238.
14. Maina PK, Shao P, Jia X, Liu Q, Umesalma S, Marin M, Long D, Jr., Concepción-Román S, Qi HH: **Histone demethylase PHF8 regulates hypoxia signaling through HIF1α and H3K4me3**. Biochim Biophys Acta Gene Regul Mech 2017, **1860**:1002–1012.
15. Eisinger-Mathason TS, Simon MC: **HIF-1alpha partners with FoxA2, a neuroendocrine-specific transcription factor, to promote tumorigenesis**. Cancer Cell 2010, **18**:3–4.
16. Park JW, Lee JK, Witte ON, Huang J: **FOXA2 is a sensitive and specific marker for small cell neuroendocrine carcinoma of the prostate**. Mod Pathol 2017, **30**:1262–1272.
17. Madeddu P: **FoxA2 hunting research identifies the early trail of mesenchymal differentiation**. Stem Cell Res Ther 2013, **4**:40.
18. Iwafuchi-Doi M, Zaret KS: **Pioneer transcription factors in cell reprogramming**. Genes Dev 2014, **28**:2679–2692.
19. Wang G, Zhao D, Spring DJ, DePinho RA: **Genetics and biology of prostate cancer**. Genes Dev 2018, **32**:1105–1140.
20. Fan L, Peng G, Sahgal N, Fazli L, Gleave M, Zhang Y, Hussain A, Qi J: **Regulation of c-Myc expression by the histone demethylase JMJD1A is essential for prostate cancer cell growth and survival**. Oncogene 2016, **35**:2441–2452.
21. Monteith GR, Davis FM, Roberts-Thomson SJ: **Calcium channels and pumps in cancer: changes and consequences**. J Biol Chem 2012, **287**:31666–31673.
22. Shin OH, Han W, Wang Y, Sudhof TC: **Evolutionarily conserved multiple C2 domain proteins with two transmembrane regions (MCTPs) and unusual Ca2 + binding properties**. J Biol Chem 2005, **280**:1641–1651.
23. Téllez-Arreola JL, Silva M, Martínez-Torres A: **MCTP-1 modulates neurotransmitter release in C. elegans**. Mol Cell Neurosci 2020, **107**:103528.

24. Tarchini B, Longo-Guess C, Tian C, Tadenev ALD, Devanney N, Johnson KR: **A spontaneous mouse deletion in Mctp1 uncovers a long-range cis-regulatory region crucial for NR2F1 function during inner ear development**. Dev Biol 2018, **443**:153–164.
25. Genc O, Dickman DK, Ma W, Tong A, Fetter RD, Davis GW: **MCTP is an ER-resident calcium sensor that stabilizes synaptic transmission and homeostatic plasticity**. Elife 2017, **6**.
26. Qiu L, Yu H, Liang F: **Multiple C2 domains transmembrane protein 1 is expressed in CNS neurons and possibly regulates cellular vesicle retrieval and oxidative stress**. J Neurochem 2015, **135**:492–507.
27. Januchowski R, Sterzynska K, Zawierucha P, Rucinski M, Swierczewska M, Partyka M, Bednarek-Rajewska K, Brazert M, Nowicki M, Zabel M, Klejewski A: **Microarray-based detection and expression analysis of new genes associated with drug resistance in ovarian cancer cell lines**. Oncotarget 2017, **8**:49944–49958.
28. Funakoshi Y, Wang Y, Semba T, Masuda H, Hout D, Ueno NT, Wang X: **Comparison of molecular profile in triple-negative inflammatory and non-inflammatory breast cancer not of mesenchymal stem-like subtype**. PLoS One 2019, **14**:e0222336.
29. Gleave M, Hsieh JT, Gao CA, von Eschenbach AC, Chung LW: **Acceleration of human prostate cancer growth in vivo by factors produced by prostate and bone fibroblasts**. Cancer Res 1991, **51**:3753–3761.
30. Chen WY, Zeng T, Wen YC, Yeh HL, Jiang KC, Chen WH, Zhang Q, Huang J, Liu YN: **Androgen deprivation-induced ZBTB46-PTGS1 signaling promotes neuroendocrine differentiation of prostate cancer**. Cancer Lett 2019, **440–441**:35–46.
31. Liu YN, Niu S, Chen WY, Zhang Q, Tao Y, Chen WH, Jiang KC, Chen X, Shi H, Liu A, et al: **Leukemia Inhibitory Factor Promotes Castration-resistant Prostate Cancer and Neuroendocrine Differentiation by Activated ZBTB46**. Clin Cancer Res 2019, **25**:4128–4140.
32. Lin SR, Wen YC, Yeh HL, Jiang KC, Chen WH, Mokgautsi N, Huang J, Chen WY, Liu YN: **EGFR-upregulated LIFR promotes SUCLG2-dependent castration resistance and neuroendocrine differentiation of prostate cancer**. Oncogene 2020.
33. Huang G, Eisenberg R, Yan M, Monti S, Lawrence E, Fu P, Walbroehl J, Lowenberg E, Golub T, Merchan J, et al: **15-Hydroxyprostaglandin dehydrogenase is a target of hepatocyte nuclear factor 3beta and a tumor suppressor in lung cancer**. Cancer Res 2008, **68**:5040–5048.
34. Genç Ö, Dickman DK, Ma W, Tong A, Fetter RD, Davis GW: **MCTP is an ER-resident calcium sensor that stabilizes synaptic transmission and homeostatic plasticity**. Elife 2017, **6**.
35. Chicas A, Wang X, Zhang C, McCurrach M, Zhao Z, Mert O, Dickins RA, Narita M, Zhang M, Lowe SW: **Dissecting the unique role of the retinoblastoma tumor suppressor during cellular senescence**. Cancer Cell 2010, **17**:376–387.
36. Elkon R, Rashi-Elkeles S, Lerenthal Y, Linhart C, Tenne T, Amariglio N, Rechavi G, Shamir R, Shiloh Y: **Dissection of a DNA-damage-induced transcriptional network using a combination of microarrays, RNA interference and computational promoter analysis**. Genome Biol 2005, **6**:R43.

37. Tomlins SA, Mehra R, Rhodes DR, Cao X, Wang L, Dhanasekaran SM, Kalyana-Sundaram S, Wei JT, Rubin MA, Pienta KJ, et al: **Integrative molecular concept modeling of prostate cancer progression**. Nat Genet 2007, **39**:41–51.
38. Ouyang X, Jessen WJ, Al-Ahmadie H, Serio AM, Lin Y, Shih WJ, Reuter VE, Scardino PT, Shen MM, Aronow BJ, et al: **Activator protein-1 transcription factors are associated with progression and recurrence of prostate cancer**. Cancer Res 2008, **68**:2132–2144.
39. Wu Y, Siadaty MS, Berens ME, Hampton GM, Theodorescu D: **Overlapping gene expression profiles of cell migration and tumor invasion in human bladder cancer identify metallothionein 1E and nicotinamide N-methyltransferase as novel regulators of cell migration**. Oncogene 2008, **27**:6679–6689.
40. Cromer A, Carles A, Millon R, Ganguli G, Chalmel F, Lemaire F, Young J, Dembélé D, Thibault C, Muller D, et al: **Identification of genes associated with tumorigenesis and metastatic potential of hypopharyngeal cancer by microarray analysis**. Oncogene 2004, **23**:2484–2498.
41. Sung SY, Hsieh CL, Law A, Zhau HE, Pathak S, Multani AS, Lim S, Coleman IM, Wu LC, Figg WD, et al: **Coevolution of prostate cancer and bone stroma in three-dimensional coculture: implications for cancer growth and metastasis**. Cancer Res 2008, **68**:9996–10003.
42. Beltran H, Rickman DS, Park K, Chae SS, Sboner A, MacDonald TY, Wang Y, Sheikh KL, Terry S, Tagawa ST, et al: **Molecular characterization of neuroendocrine prostate cancer and identification of new drug targets**. Cancer Discov 2011, **1**:487–495.
43. Palmgren JS, Karavadia SS, Wakefield MR: **Unusual and underappreciated: small cell carcinoma of the prostate**. Semin Oncol 2007, **34**:22–29.
44. Lovnicki J, Gan Y, Feng T, Li Y, Xie N, Ho CH, Lee AR, Chen X, Nappi L, Han B, et al: **LIN28B promotes the development of neuroendocrine prostate cancer**. J Clin Invest 2020, **130**:5338–5348.
45. Davis FM, Azimi I, Faville RA, Peters AA, Jalink K, Putney JW, Jr., Goodhill GJ, Thompson EW, Roberts-Thomson SJ, Monteith GR: **Induction of epithelial-mesenchymal transition (EMT) in breast cancer cells is calcium signal dependent**. Oncogene 2014, **33**:2307–2316.
46. Song J: **Targeting epithelial-mesenchymal transition pathway in hepatocellular carcinoma**. Clin Mol Hepatol 2020, **26**:484–486.
47. Bery F, Cancel M, Chantome A, Guibon R, Bruyere F, Rozet F, Maheo K, Fromont G: **The Calcium-Sensing Receptor is A Marker and Potential Driver of Neuroendocrine Differentiation in Prostate Cancer**. *Cancers (Basel)* 2020, **12**.
48. Silvestri R, Pucci P, Venalainen E, Matheou C, Mather R, Chandler S, Aceto R, Rigas SH, Wang Y, Rietdorf K, et al: **T-type calcium channels drive the proliferation of androgen-receptor negative prostate cancer cells**. Prostate 2019, **79**:1580–1586.
49. Kong L, Yang W, Chen L, Qian L: **The DNA methylation-regulated MCTP1 activates the drug-resistance of esophageal cancer cells**. Aging (Albany NY) 2021, **13**:3342–3352.
50. Qi J, Nakayama K, Cardiff RD, Borowsky AD, Kaul K, Williams R, Krajewski S, Mercola D, Carpenter PM, Bowtell D, Ronai ZA: **Siah2-dependent concerted activity of HIF and FoxA2 regulates formation**

of neuroendocrine phenotype and neuroendocrine prostate tumors. Cancer Cell 2010, **18**:23–38.

51. Patel GK, Chugh N, Tripathi M: **Neuroendocrine Differentiation of Prostate Cancer-An Intriguing Example of Tumor Evolution at Play**. Cancers (Basel) 2019, **11**:1405.
52. Ming L, Byrne NM, Camac SN, Mitchell CA, Ward C, Waugh DJ, McKeown SR, Worthington J: **Androgen deprivation results in time-dependent hypoxia in LNCaP prostate tumours: informed scheduling of the bioreductive drug AQ4N improves treatment response**. Int J Cancer 2013, **132**:1323–1332.
53. Tajada S, Villalobos C: **Calcium Permeable Channels in Cancer Hallmarks**. Front Pharmacol 2020, **11**:968.
54. Bose T, Cieślar-Pobuda A, Wiechec E: **Role of ion channels in regulating Ca²â□º homeostasis during the interplay between immune and cancer cells**. Cell Death Dis 2015, **6**:e1648.
55. Burgoyne RD, Helassa N, McCue HV, Haynes LP: **Calcium Sensors in Neuronal Function and Dysfunction**. Cold Spring Harb Perspect Biol 2019, **11**.
56. Shin OH, Han W, Wang Y, Südhof TC: **Evolutionarily conserved multiple C2 domain proteins with two transmembrane regions (MCTPs) and unusual Ca2 + binding properties**. J Biol Chem 2005, **280**:1641–1651.
57. Bhattacharya A, Kumar J, Hermanson K, Sun Y, Qureshi H, Perley D, Scheidegger A, Singh BB, Dhasarathy A: **The calcium channel proteins ORAI3 and STIM1 mediate TGF-beta induced Snai1 expression**. Oncotarget 2018, **9**:29468–29483.
58. Zechner D, Fujita Y, Hulsken J, Muller T, Walther I, Taketo MM, Crenshaw EB, 3rd, Birchmeier W, Birchmeier C: **beta-Catenin signals regulate cell growth and the balance between progenitor cell expansion and differentiation in the nervous system**. Dev Biol 2003, **258**:406–418.
59. McKeithen D, Graham T, Chung LW, Odero-Marah V: **Snail transcription factor regulates neuroendocrine differentiation in LNCaP prostate cancer cells**. Prostate 2010, **70**:982–992.
60. Tsang ML: **Chemotherapy and Prostate Cancer**. In *Chemotherapy and Immunotherapy in Urologic Oncology.* 2021: 105–118

Figures

Figure 1

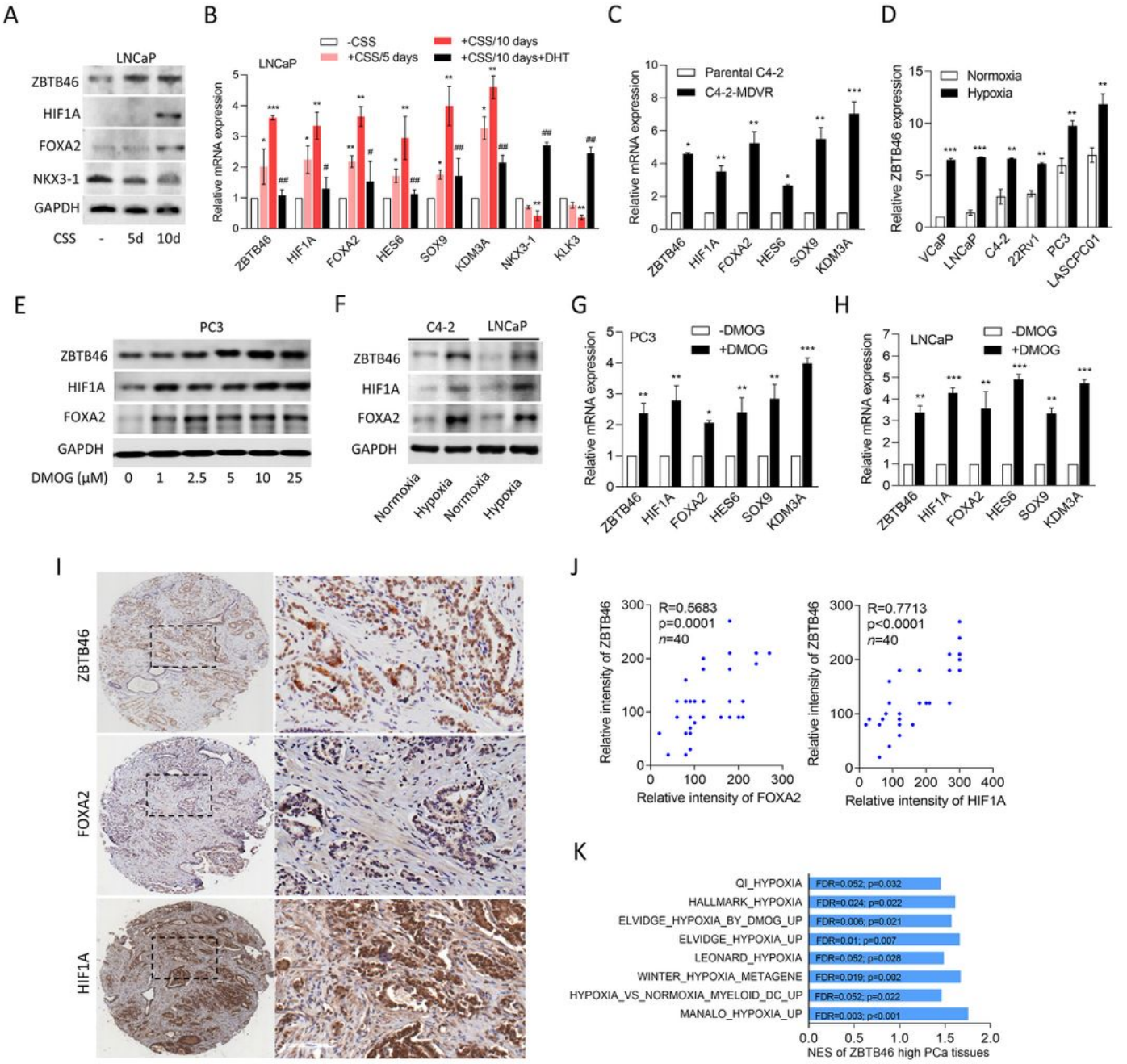

Figure 1

ADT-induced ZBTB46 is associated with HIF1A/FOXA2 upregulation. **A** Western blotting to determine ZBTB46, HIF1A, FOXA2, and NKX3-1 in LNCaP cells cultured in 10% CSS-containing medium for the indicated days. **B** Relative mRNA levels of ZBTB46, HIF1A, FOXA2, HES6, SOX9, KDM3A, NKX3-1, and KLK3 in LNCaP cells with 5 or 10 days of 10% CSS-containing medium treatment and further treated with 10 nM DHT for 24 h. * vs. -CSS; # vs. +CSS/10 days, by a two-way ANOVA. **C** Relative mRNA levels of

ZBTB46, HIF1A, FOXA2, HES6, SOX9, KDM3A, NKX3-1, and KLK3 in parental C4-2 cells compared to C4-2-MDVR cells. * vs. Parental C4-2, by a one-way ANOVA. **D** Relative mRNA levels of ZBTB46 in a panel of PCa cell lines cultured in normoxia (21% O_2) and hypoxia (1% O_2) for 24 h. * vs. Normoxia, by a one-way ANOVA. **E** ZBTB46, HIF1A, and FOXA2 protein levels in PC3 cells treated with various concentrations of DMOG for 24 h. **F** ZBTB46, HIF1A, and FOXA2 protein levels in C4-2 and LNCaP cells cultured in normoxia (21% O_2) and hypoxia (1% O_2) for 24 h. **G** and **H** Relative mRNA levels of ZBTB46, HIF1A, FOXA2, HES6, SOX9, and KDM3A in PC3 (**G**) and LNCaP (**H**) cells treated with 10 μM DMOG for 24 h. * vs. -DMOG, by a one-way ANOVA. Quantification of mRNA is presented as the mean ± SEM from three biological replicates. * $p<0.05$, ** $p<0.01$, *** $p<0.001$. **I** and **J** IHC staining (**I**) and relative intensities (**J**) of ZBTB46, HIF1A, and FOXA2 of the CA4 PCa TMA. The significance of the positive correlations among the intensities of ZBTB46, FOXA2, and HIF1A was determined by two-tailed Pearson correlation XY analyses using GraphPad Prism. *R*, correlation coefficient, *P*, *p* (two-tailed) value. **K** GSEA of TCGA PCa database showing the enrichment of ZBTB46 expression associated with upregulated expression of hypoxia-responsive gene signatures. NES, normalized enrichment score; FDR, false discovery rate.

Figure 2

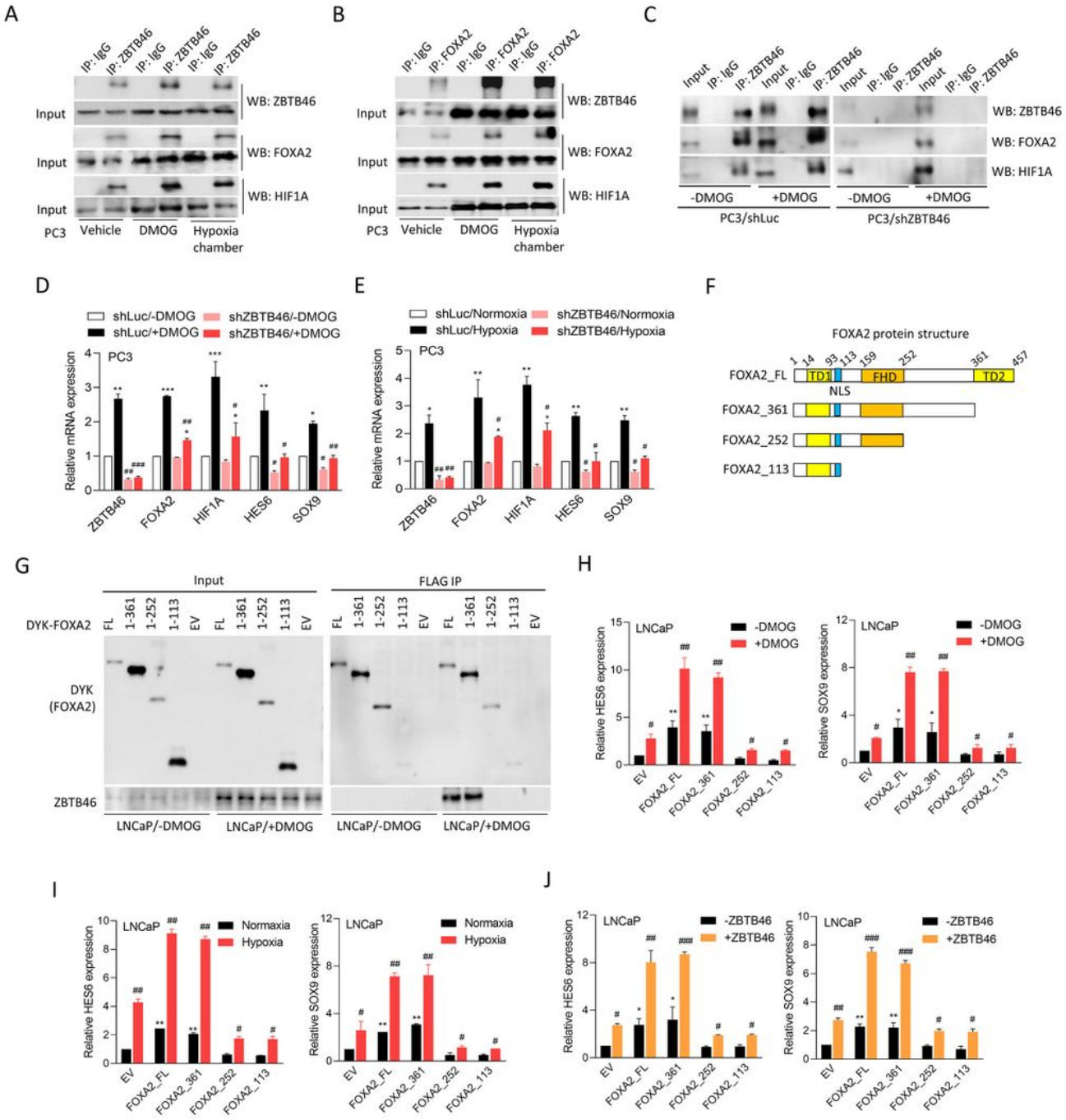

Figure 2

ZBTB46 potentially interacts with the HIF1A and FOXA2 protein complex. **A** and **B** IP of ZBTB46 (A), FOXA2 (B) or IgG, and WB of ZBTB46, FOXA2, and HIF1A proteins in PC3 cells cultured with 10 μM of DMOG or in a hypoxic chamber for 24 h. **C** IP of ZBTB46 or IgG, and WB of ZBTB46, FOXA2, and HIF1A proteins in PC3 cells harboring a non-target control (Luc) or ZBTB46-KD shRNA vector following cultured with 10 μM of DMOG for 24 h. **D** and **E** Relative mRNA levels of ZBTB46, FOXA2, HIF1A, HES6, and SOX9

in PC3 cells expressing Luc or ZBTB46-KD shRNA vector following treatment with 10 μM DMOG (**D**) or cultured in hypoxia (1% O_2) condition (**E**) for 24 h. * vs. -DMOG (**D**) or normoxia (**E**); # vs. shLuc, by a two-way ANOVA. **F** Various truncation mutants of FOXA2 protein constructs. **G** IP of DYK for DYK-tagged FOXA2 mutants, and WB of ZBTB46 or DYK for various FOXA2 mutants in LNCaP cells co-transfected with full-length ZBTB46 and DYK-tagged FOXA2 mutants expression vector following cultured with 10 μM of DMOG for 24 h. **H-J** Relative mRNA levels of hypoxia-related gene (*HES6* and *SOX9*) in LNCaP cells transfected with an empty vector (EV), wild type (FOXA2_FL) or various mutants of the FOXA2 expression vector following cultured in 10 μM DMOG (**H**) or hypoxia (1% O_2) condition (**I**) for 24 h or co-transfected with ZBTB46 cDNA vector (**J**). * vs. the EV; # vs. -DMOG (**H**), Nomaxia (**I**) or -ZBTB46 (**J**), by a two-way ANOVA. Quantification of mRNA is presented as the mean ± SEM from three biological replicates. * $p<0.05$, ** $p<0.01$, *** $p<0.001$.

Figure 3

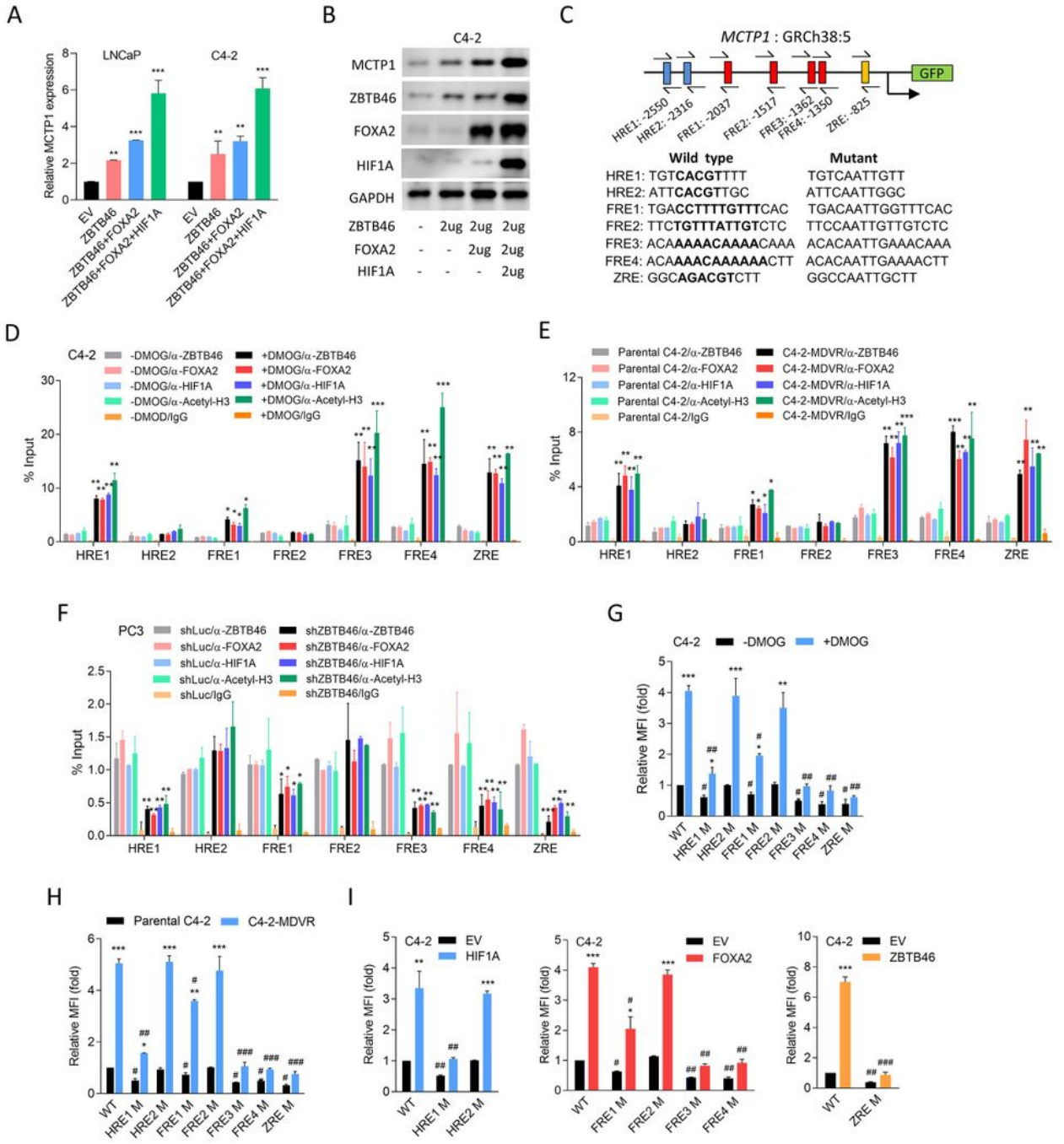

Figure 3

ZBTB46/FOXA2/HIF1A complex transcriptionally drives *MCTP1* after ADT. **A** and **B** mRNA levels of MCTP1 in LNCaP and C4-2 cells (**A**) and protein levels of MCTP1, ZBTB46, FOXA2, and HIF1A in C4-2 cells (**B**) transiently transfected with an empty vector (EV), or ZBTB46, FOXA2, and HIF1A cDNA vector. * vs. the EV, by a one-way ANOVA. Quantification of mRNA is presented as the mean ± SEM from three biological replicates. ** p<0.01, *** p<0.001. **C** Schematic of the predicted HIF1A-, FOXA2-, and ZBTB46-

response elements (HRE, FRE, and ZRE) and various introduced binding site mutants in regulatory sequence reporter constructs of human *MCTP1* (GRCh38:5); and sequence diagram of wild-type (WT) and mutant (M) HRE, FRE, and ZRE. **D-F** ChIP assay showing binding of ZBTB46, FOXA2, and HIF1A compared to acetyl-H3 to the predicted HRE, FRE, and ZRE of the *MCTP1* gene regulatory sequence in C4-2 cells treated with 10 μM DMOG for 24 h (**D**) or in parental C4-2 or C4-2-MDVR cells (**E**) or in PC3 cells following stable transfection with a non-target control (Luc) or the ZBTB46 shRNA vector (**F**). Sheared chromatin from nuclear extracts was precipitated with antibodies against ZBTB46, FOXA2, HIF1A, and acetyl-H3, and predictive primers (**C**, black arrows) were used to quantify the precipitated DNA by a qPCR. Enrichment of each protein to each site is given as a percentage of the total input and then normalized to IgG. * vs. -DMOG (**D**) or parental C4-2 cells (**E**) or shLuc (**F**); by a one-way ANOVA. **G** and **H** Relative MFI of the GFP reporter gene containing WT and M from the *MCTP1* regulatory sequence in C4-2 cells following 10 μM DMOG treatment for 24 h (**G**) or in parental C4-2 or C4-2-MDVR cells (**H**). * vs. -DMOG (**G**) or parental C4-2 cells (**H**); $^{\#}$ vs. WT, by a two-way ANOVA. **I** Relative MFI of the GFP reporter gene containing WT and M from the *MCTP1* regulatory sequence in C4-2 cells transiently transfected with the EV, ZBTB46, FOXA2, or HIF1A cDNA vector. * vs. the EV; $^{\#}$ vs. WT, by a two-way ANOVA. Quantification of the ChIP assay and relative MFI values are presented as the mean ± SEM from three biological replicates. * $p<0.05$, ** $p<0.01$, *** $p<0.001$.

Figure 4

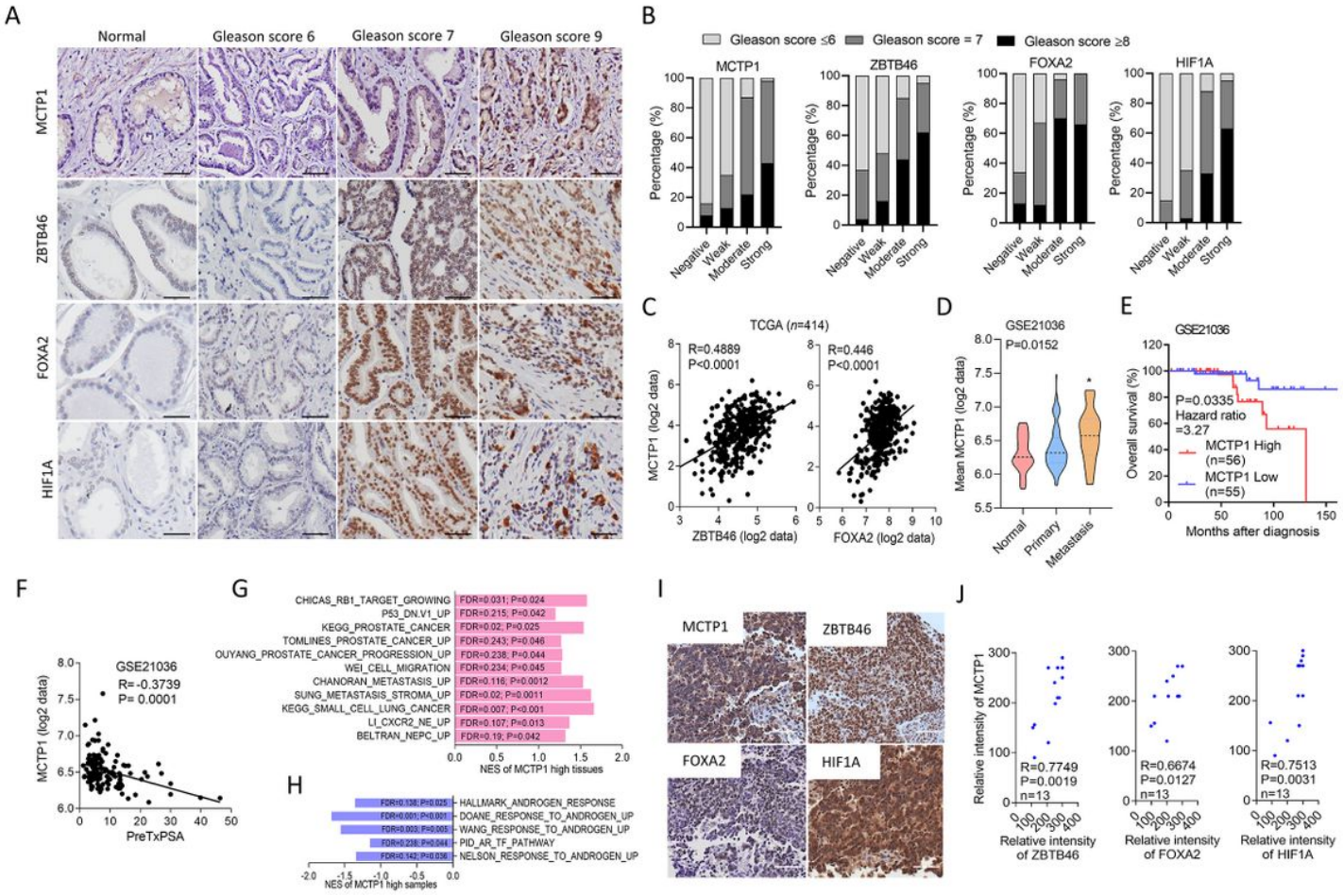

Figure 4

MCTP1 is upregulated in high-grade PCa and NEPC tumors. **A** IHC staining of MCTP1, ZBTB46, FOXA2, and HIF1A in a primary PCa TMA collected from the Duke University School of Medicine (Durham, NC, USA). Scale bars, 100 μm. **B** Statistical analysis of the percentage and intensity of MCTP1, ZBTB46, FOXA2, and HIF1A. Intensities were semiquantitatively scored using the H-index as follows: negative, weakly positive, moderately positive, and strongly positive. *p* values were calculated by a Chi-squared test performed using SPSS statistical 18.0 software. $p<0.001$. **C** Pearson correlation coefficient analysis of mean mRNA expression of MCTP1 relative to ZBTB46 and FOXA2 in patients ($n=414$) from TCGA PCa dataset. **D** Mean mRNA expression of MCTP1 in human normal ($n=28$), primary ($n=98$), and metastatic ($n=13$) prostate samples from the GSE21035 PCa dataset. * vs. normal tissues. * $p<0.05$; one-way ANOVA. **E** Kaplan-Meier analyses of MCTP1 levels in the GSE21035 PCa dataset. Significance was determined by a log-rank (Mantel Cox) test. $p=0.0335$; Hazard ratio (MCTP1 high/MCTP1 low) =3.27. **F** Pearson correlation coefficient analysis of mean MCTP1 levels relative to PSA serum levels in patients ($n=111$) from the GSE21035 PCa dataset. **G** and **H** GSEA of TCGA PCa dataset showed that higher

MCTP1 expression of prostate tissues was positively associated with malignant progression and NEPC-responsive gene signatures (**G**) or negatively associated with androgen-responsive gene signatures (**H**). NES, normalized enrichment score; FDR, false discovery rate. **I** and **J** IHC staining (**I**) and relative intensities (**J**) of MCTP1, ZBTB46, HIF1A, and FOXA2 of the SCPC TMA collected from the Duke University School of Medicine. The significance of the positive correlation among the intensities of MCTP1, ZBTB46, FOXA2, and HIF1A was determined by two-tailed Pearson correlation XY analyses in GraphPad Prism. *R*, correlation coefficient, *P*, p (two-tailed) value.

Figure 5

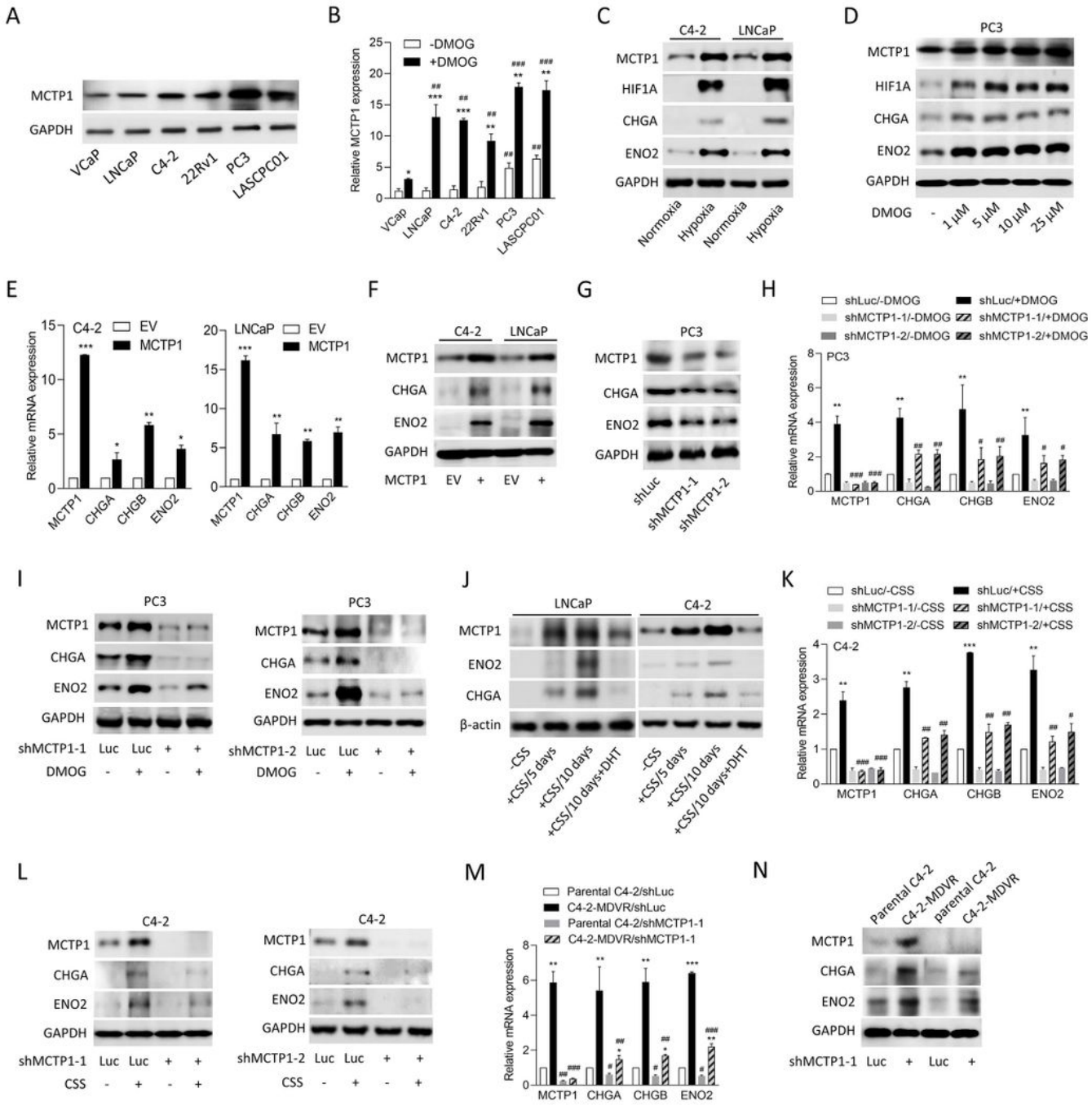

Figure 5

MCTP1 stimulation is associated with NED and is upregulated in PCa after ADT. **A** Relative protein levels of MCTP1 in a panel of PCa cell lines. **B** Relative mRNA levels of MCTP1 in various PCa cells following 10 μM DMOG treatment for 24 h. * vs. -DMOG; # vs. VCaP, by a two-way ANOVA. **C** MCTP1, HIF1A, CHGA, and ENO2 protein levels in C4-2 and LNCaP cells cultured in normoxia (21% O_2) and hypoxia (1% O_2) for 24 h. **D** WB of MCTP1, HIF1A, CHGA, and ENO2 in PC3 cells treated with various concentrations of DMOG for 24 h. **E** and **F** Relative mRNA (**E**) and protein (**F**) levels of MCTP1 and NE markers in C4-2 and LNCaP cells following stable transfection with an empty vector (EV) or an MCTP1 cDNA vector. * vs. the EV, by a one-way ANOVA. **G** Relative protein levels of MCTP1 and NE markers in PC3 cells following stable transfection with non-target control (Luc) or an MCTP1 shRNA vector. **H** and **I** Relative mRNA (**H**) and protein (**I**) levels of MCTP1 and NE markers in PC3 cells expressing Luc or an MCTP1 shRNA vector following treatment with 10 μM DMOG for 24 h. * vs. -DMOG; # vs. shLuc, by a two-way ANOVA. **J** Relative protein levels of MCTP1, ENO2, and CHGA in LNCaP and C4-2 cells following treatment with CSS-containing medium for 5 and 10 days and 10 nM DHT for 24 h. **K** and **L** Relative mRNA (**K**) and protein (**L**) levels of MCTP1 and NE markers in C4-2 cells expressing control or MCTP1-KD following treatment with CSS-containing medium for 5 days. * vs. -CSS; # vs. shLuc, by a two-way ANOVA. **M** and **N** Relative mRNA (**M**) and protein (**N**) levels of MCTP1 and NE markers in parental C4-2 cells compared to MDV3100-resistant C4-2 cells following transfected with control or an MCTP1 shRNA vector. * vs. parental C4-2; # vs. shLuc, by a two-way ANOVA. Quantification of mRNA is presented as the mean ± SEM from three biological replicates. * $p<0.05$, ** $p<0.01$, *** $p<0.001$.

Figure 6

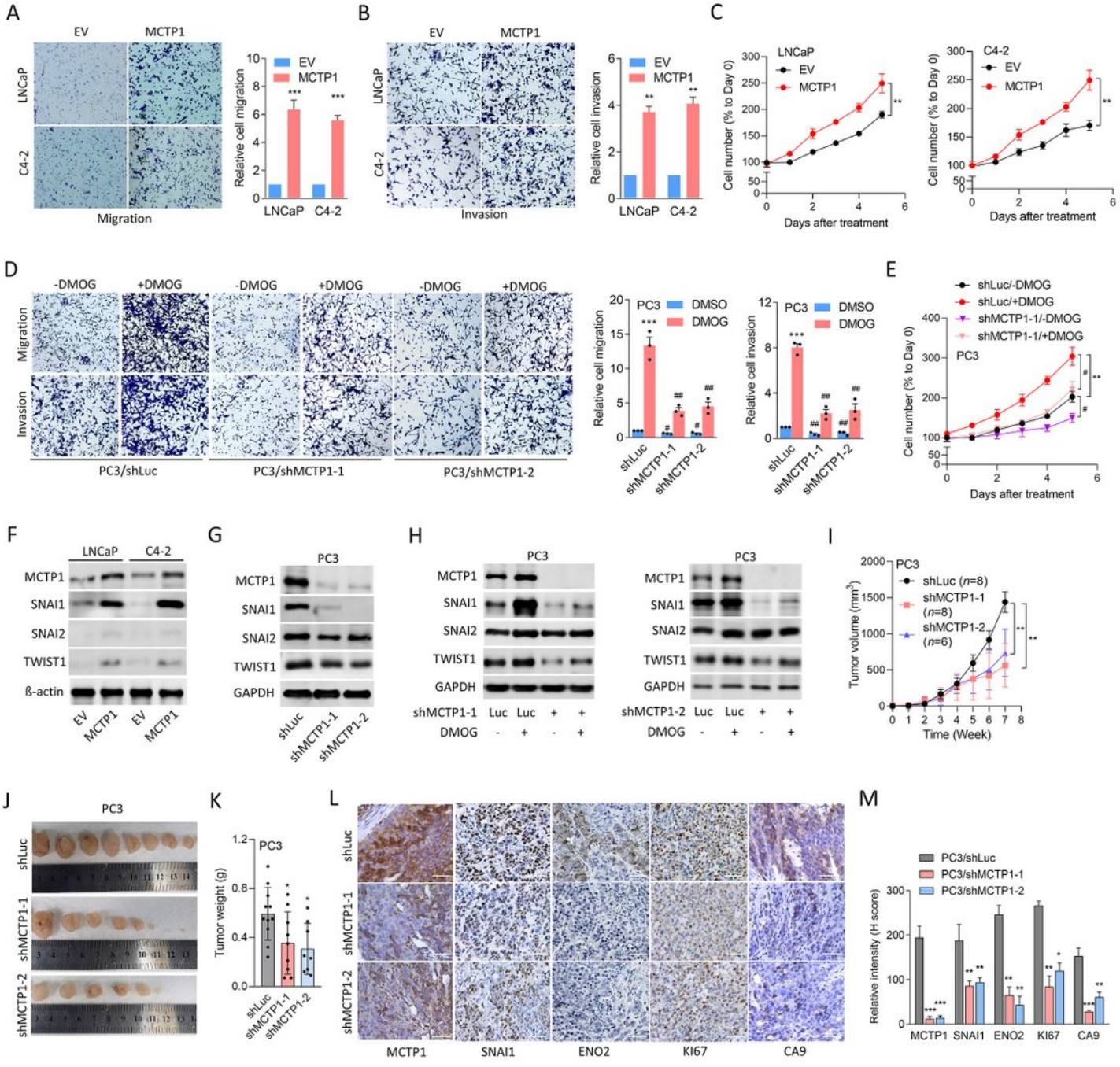

Figure 6

Hypoxia-induced MCTP1 promotes malignant cell progression. **A-C** Relative migration and invasion (**A** and **B**) and proliferation (**C**) of LNCaP and C4-2 cells stably transfected with an empty vector (EV) or an MCTP1 cDNA vector. *n*=5 per group. * vs. the EV, by a one-way ANOVA. **D** and **E** Relative migration and invasion (**D**) and proliferation (**E**) of PC3 cells stably transfected with a non-target control (Luc) or an MCTP1 shRNA vector following treatment with 10 μM DMOG for 24 h. *n*=5 per group. * vs. -DMOG; # vs.

shLuc, by a two-way ANOVA. Quantification of migration, invasion, and proliferation assays presented as the mean ± SEM from three biological replicates. * p<0.05, ** p<0.01, *** p<0.001. **F** Protein levels of MCTP1, SNAI1, SNAI2, and TWIST1 in LNCaP and C4-2 cells stably expressing an EV or MCTP1 cDNA vector. **G** Protein levels of MCTP1, SNAI1, SNAI2, and TWIST1 in PC3 cells stably transfected with the Luc or MCTP1 shRNA vector. **H** Protein levels of MCTP1, SNAI1, SNAI2, and TWIST1 in PC3 cells expressing control or MCTP1-KD following treatment with 10 μM DMOG for 24 h. **I-K** Tumor growth analysis of mice subcutaneously inoculated with PC3 cells harboring the Luc or MCTP1 shRNA vector. Tumor sizes were monitored once a week (**I**), and images (**J**) and tumor weights (**K**) were obtained at the end of the experiment. * vs. shLuc. * p<0.05, ** p<0.01, by a one-way ANOVA. **L** and **M** IHC staining (**L**) and representative intensities (**M**) of MCTP1, SNAI1, ENO2, KI67, and CA9 in subcutaneous tumors from (**J**). * vs. shLuc. Significance was determined by a two-tailed Student's *t*-test. * p<0.05, ** p<0.01.

Figure 7

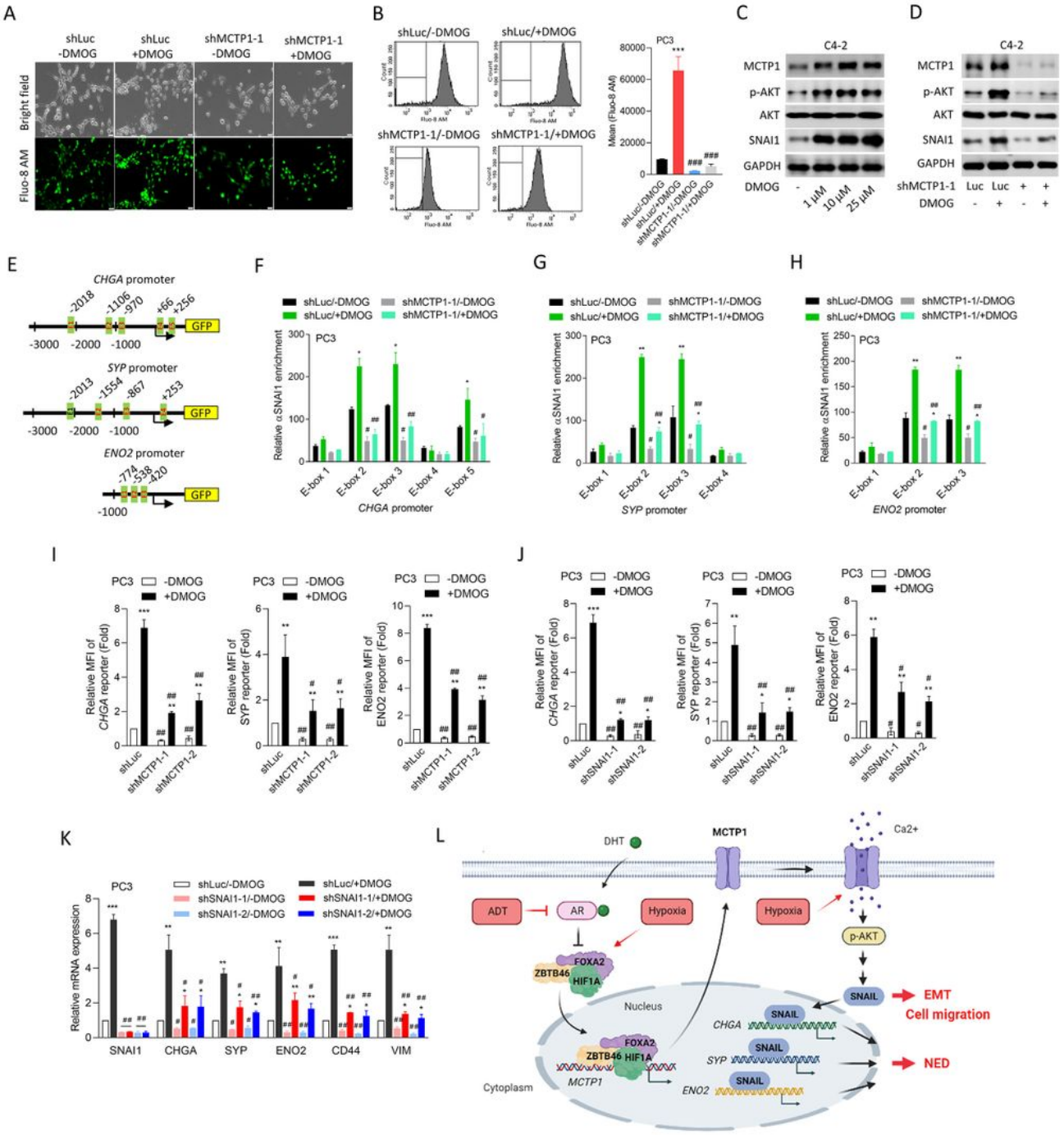

Figure 7

Hypoxia-induced MCTP1 stabilize SNAI1 and drives NED and EMT of PCa through a calcium-activated AKT signaling. **A** Fluorescent imaging the calcium in PC3 cells expressing a non-target control (Luc) or MCTP1 shRNA vector following treatment with 10 μM DMOG for 24 h in calcium-free Hank's balanced salt solution (HBSS) and were labeled with Fluo-8 AM and examined under a fluorescent microscope. **B** Flow cytometry analysis of calcium in PC3 cells expressing Luc or MCTP1 shRNA vector following

treatment with 10 μM DMOG for 24 h in calcium-free HBSS after labeled with Fluo-8 AM. **C** Protein levels of MCTP1, phosphorylated-AKT, AKT, and SNAI1 in C4-2 cells treatment with 0, 1, 10, and 25 μM of DMOG for 24 h. **D** Protein levels of MCTP1, phosphorylated-AKT, AKT, and SNAI1 in C4-2 cells stably transfected Luc or MCTP1 shRNA vector following treatment with 10 μM DMOG for 24 h. **E** Schematic of the predicted E-box in the regulatory sequence of the human *CHGA*, *SYP*, and *ENO2* genes. **F-H** ChIP assay showing binding of nuclear SNAI1 to predicted E-boxes of *CHGA*, *SYP*, and *ENO2* genes regulatory sequence in PC3 cells stably transfected Luc or MCTP1 shRNA vector following treatment with 10 μM DMOG for 24 h. Sheared chromatin from nuclear extracts was precipitated with antibody against SNAI1, and predictive primers for putative E-boxes (**E**) were used to quantify the precipitated DNA by a qPCR. Enrichment of each protein to each site is given as a percentage of the total input and then normalized to IgG. * vs. -DMOG; # vs. shLuc. Data from relative ChIP enrichment levels are the mean ± SEM of three independent experiments. * $p < 0.05$, ** $p < 0.01$, and *** $p < 0.001$ by a two-way ANOVA. **I** and **J** Relative MFI of the GFP reporter gene containing the *CHGA*, *SYP*, and *ENO2* regulatory sequences in PC3 cells stably transfected with Luc, MCTP1-KD (**I**) or SNAI1-KD (**J**) shRNA vector following treatment with 10 μM DMOG for 24 h. n=3 per group. * vs. -DMOG; # vs. shLuc, by a two-way ANOVA. **K** Relative mRNA levels of SNAI1, NE (CHGA, SYP, and ENO2), and EMT (CD44 and VIM) markers in PC3 cells expressing Luc or SNAI1-KD shRNA vector following treatment with 10 μM DMOG for 24 h. * vs. -DMOG; # vs. shLuc, by a two-way ANOVA. Quantification of mRNA and relative MFI are presented as the mean ± SEM from three biological replicates. * $p<0.05$, ** $p<0.01$, *** $p<0.001$. **L** Proposed model for ADT-mediated NED links with the hypoxia-induced FOXA2/HIF1A/ZBTB46 pathway through upregulation of MCTP1 in PCa. The effect of MCTP1 on the enhancement of the EMT and NEPC development through the upregulation of SNAI1-driven EMT and NE markers by activating the calcium-activated AKT signaling.

Supplementary Files

This is a list of supplementary files associated with this preprint. Click to download.

- Additionalfile1.docx